

Master's thesis



**Ytterbium-doped Mode Locked
Fiber Laser via Pump Modulation**
(ポンプ変調を用いたイッテルビウム
ドープモード同期ファイバレーザ)

Supervisor: Professor Shinji Yamashita

Author: Zihao Zhao

Student ID number: 37-175098

Graduate School of Engineering

Department of Electrical Engineering and Information Systems

August 15, 2019

Contents

Contents	i
List of Figures	iii
1 Introduction	1
1.1 Mode Locked Fiber Lasers	1
1.2 Application of Mode Locked Fiber Lasers	2
1.3 Purpose and Organization of this thesis	2
2 Fundamentals of Mode Locked Fiber Lasers	3
2.1 Principle of Mode Locking	3
2.2 Mode Locking Techniques	4
2.2.1 Active Mode Locking	4
2.2.2 Passive Mode Locking	5
2.3 Pulse Propagation in Optical Fiber	8
2.4 Pulse Shaping at Anomalous Dispersion and Normal Dispersion	12
2.5 Simulation Method	12
3 Pump to Signal Transfer of Modulation Index in Gain Fiber	15
3.1 Theoretical Model of Gain Modulation	15
3.2 Experimental Measurement of Pump to Signal Transfer	18
3.3 Conclusion	25
4 Active Mode Locking via Pump Modulation	27
4.1 Introduction	27
4.2 Previous Work on Active Mode Locking via Pump Modulation	28
4.2.1 Thulium-doped Mode Locked Fiber Laser via Pump Modulation	28
4.2.2 Erbium-doped Mode Locked Fiber Laser via Pump Modulation	29
4.3 Ytterbium Doped Mode Locked Fiber Laser via Pump Modulation	31
4.3.1 All Normal Dispersion Configuration	32
4.3.2 All Normal Dispersion Configuration with Kilometer-long Cavity	38
4.3.3 Dispersion Compensated Configuration	40
4.3.4 Conclusion	41

5 Conclusion and Future Work	43
5.1 Conclusion	43
5.2 Future Work	43
Appendix	45
Pulse Propagation Equation	45
MATLAB code for simulating pulse propagation in gain fiber	47
Dispersion Compensation with Grating Pair	48
Acknowledgments	49
Bibliography	51

List of Figures

2.1	Schematic of a linear laser cavity	3
2.2	Schematic of active mode locking by amplitude modulation	4
2.3	Active mode locking by amplitude modulation in time domain	5
2.4	Active mode locking by amplitude modulation in frequency domain	5
2.5	Saturable absorber	6
2.6	Schematic of passive mode locking	6
2.7	Typical schematic of NPR mode locked fiber laser	7
2.8	Schematic of nonlinear amplifying loop mirror	7
2.9	Typical schematic of NALM mode locked fiber laser	8
2.10	Carbon nanotube [22]	8
2.11	Dispersion parameter with wavelength for a single-mode fiber [23]	10
2.12	Fiber loss with wavelength. Dashed curve shows the loss resulted from Rayleigh scattering [23].	10
3.1	Three-level system	16
3.2	Experimental setup for measuring pump to signal transfer T in Yb-doped fiber	19
3.3	Transfer T at different saturation level in Yb-doped fiber. Dotted line: experimental measurements; solid line: simulations; inset: gain saturation.	20
3.4	Transfer T at different pumping level in Yb-doped fiber. Dotted line: experimental measurements; solid line: simulations.	21
3.5	Experimental setup for measuring pump to signal transfer T in Tm-doped fiber	22
3.6	Transfer T at different saturation level in Tm-doped fiber. Dotted line: experimental measurements; solid line: simulations, inset: gain saturation.	23
3.7	Transfer T at different pumping level in Tm-doped fiber. Dotted line: experimental measurements; solid line: simulations.	23
3.8	Experimental setup for measuring pump to signal transfer T in Er-doped fiber	24
3.9	Transfer T at different saturation level in Er-doped fiber. Dotted line: experimental measurements; solid line: simulations, inset: gain saturation.	24
3.10	Transfer T at different pumping level in Er-doped fiber. Dotted line: experimental measurements; solid line: simulations.	25
4.1	Schematic of active mode locking by pump modulation	27
4.2	Active mode locking by pump modulation in time domain	28

4.3	Active mode locking via pump modulation in Tm-doped fiber laser [16]	28
4.4	Experiment results. (a) Output spectrum; (b) autocorrelation trace (inset: oscilloscope waveform); (c) and (d) RF spectrum. [16]	29
4.5	Second-harmonic mode locking experiment results. (a) Output spectrum; (b) autocorrelation trace (inset: oscilloscope waveform); (c) and (d) RF spectrum. [16]	30
4.6	Active mode locking via pump modulation in Tm-doped fiber laser [17]	31
4.7	Experiment results. (a) Output spectrum; (b) PF spectrum; (c) autocorrelation trace. [17]	31
4.8	Experimental setup for all normal dispersion configuration	32
4.9	Flow diagram of the simulation	33
4.10	Simulation result: pulse shape when modulation index $m = 1/2^i$, $i = 0, 1, 2, \dots, 6$	34
4.11	Simulation result: spectrum when modulation index $m = 1/2^i$, $i = 0, 1, 2, \dots, 6$	35
4.12	Simulation result: pulse shape when modulation index $m = 1/2^i$, $i = 7, 8, 9, 10$	35
4.13	Simulation result: spectrum when modulation index $m = 1/2^i$, $i = 7, 8, 9, 10$	36
4.14	Simulation result: temporal output when modulation index $m = 1/2^i$, $i = 11, 12, 13, 14$	36
4.15	Simulation result: spectrum when modulation index $m = 1/2^i$, $i = 11, 12, 13, 14$	37
4.16	Experimental setup for all normal dispersion configuration with kilometer-long cavity	37
4.17	Output pulse measured by PD and oscilloscope. Pulse width: 500 ns	38
4.18	Output spectrum. 3 dB bandwidth: 2.5 nm	39
4.19	Spectrum (left) and normalized temporal shape (right) before (blue) and after (red) passing through 500 m SMF-28	39
4.20	Experimental setup for dispersion compensated configuration	40
4.21	One frame of unstable pulse train footage	41
5.1	Grating pair for dispersion compensation	48

Chapter 1

Introduction

1.1 Mode Locked Fiber Lasers

Laser is one of the greatest human inventions. It can generate the purest light with high coherence that does not originally exist in nature. Lasers can be classified into two categories by their operation mode: continuous wave (CW) laser and pulsed laser. Output of a CW laser is constant over time while output of a pulsed laser exhibits as a pulse train in time domain. There are a few common techniques to realize pulsed laser, such as Q-switching [1] and mode-locking [2]. Q-switch laser usually generates pulses with microsecond to nanosecond pulse width. Mode-locked laser is capable of generating pulses with picosecond to femtosecond pulse width, which are often referred as ultrashort pulses nowadays. Ultrashort pulsed laser has extremely high peak intensity and ultrashort temporal resolution compared to CW lasers. This thesis mainly focuses on mode locked fiber lasers.

Mode locked fiber laser is of great interest because of its outstanding advantages and versatility such as:

- (1) Fiber laser is compact compared to other lasers such as solid-state laser, since fiber is flexible enough to be coiled;
- (2) Fiber laser is easy to fabricate compared to free space laser which requires highly precise alignment, whereas fiber laser can be fabricated by only fiber splicing;
- (3) Fiber laser can be easily delivered to any moving elements since the laser is originally generated in optical fiber. This advantage makes it widely applied to laser machining;
- (4) Fiber laser costs lower than other laser sources of comparable performance such as solid-state laser.

For mode locked fiber lasers, there are mainly three types by their gain medium: erbium (Er), ytterbium (Yb) and thulium (Tm) doped fiber laser, with central wavelength of $1.5 \mu m$, $1 \mu m$ and $2 \mu m$ respectively. They are widely applied in different field based on their operation wavelength. Er-doped fiber laser are widely used in telecommunication because of fiber exhibits minimum loss at $1.5 \mu m$. Yb-doped fiber laser are suitable for high power operation because of high quantum efficiency of ytterbium ion [3]. Tm-doped fiber laser is "eye-safe" laser because of moderate water absorption at $2 \mu m$ [4], offering great potential in fields like laser imaging detection and ranging (LIDAR) and gas sensing systems.

1.2 Application of Mode Locked Fiber Lasers

Mode locked fiber laser has a variety of applications because of its high temporal/spatial resolution and high peak intensity, such as:

Ultrashort laser spectroscopy

Ultrashort laser spectroscopy is a technique for studying dynamics in an extremely short time scale, taking the advantage of high temporal resolution of ultrashort laser [5, 6]. Ultrashort pulses play the role as a high frame camera in the process. It is widely applied in the study of atom and molecule dynamics.

Biomedical imaging

Thanks to its high peak intensity, mode locked fiber laser can also be applied for biomedical imaging such as stimulated Raman scattering microscopy [7] and multiphoton microscopy [8, 9]. In multiphoton microscopy, the fluorophore excites when multiple incident photons hit the fluorophore simultaneously, resulting the emission of light for microscopy. High peak intensity can greatly increase the probability of multiple photons hit the fluorophore simultaneously.

Ultrashort laser micromachining

High quality micromachining requires ultrashort laser instead of CW laser [10, 11]. In an ultrashort laser machining, energy is deposited onto the material so fast that the material will turn into a plasma state rather than melting down. Residual heat dissipates away immediately with the plasma, leaving a clean micromachining spot.

1.3 Purpose and Organization of this thesis

To date, there are various widely applied techniques for mode locking a fiber laser. Mainstream saturable absorbers for mode locking include semiconductor saturable absorber mirror (SESAM) [12], nonlinear polarization rotation (NPR) [13], nonlinear loop mirror (NOLM) [14] and carbon nanotube (CNT) [15], etc. In this thesis, we focus on a novel mode locking technique called active mode locking via pump modulation (AMPM). As Tm [16] and Er-doped mode locked fiber laser by AMPM [17] have been achieved previously in our lab, this thesis mainly focuses on the study of Yb-doped mode locked fiber laser with the technique of AMPM.

Chapter 2 introduces the fundamentals of mode locked fiber lasers, including the principle of mode locking, mode locking techniques, pulse propagation in optical fiber, pulse shaping at different dispersion regime and simulation method. Chapter 3 shows the theoretical model and experimental measurements for pump to signal transfer in gain fiber. This is the ground stone of the AMPM technique. In chapter 4, we firstly introduce the concept and principle of AMPM and previous work on Tm and Er-doped mode locked fiber laser by AMPM. Then, we move on to the experiments of Yb-doped mode locked fiber laser by AMPM. We present our experimental setups, results and analysis. Chapter 5 includes the conclusion of the whole thesis and future work regarding the method of pump modulation.

Chapter 2

Fundamentals of Mode Locked Fiber Lasers

2.1 Principle of Mode Locking

Mode locking is a technique for generating ultrashort laser pulses [18]. The term "mode locking" means the phase relation of longitudinal modes of the laser cavity is fixed. In this case, the superposition of the longitudinal modes becomes a short pulse trains. For a detailed explanation, here we firstly introduce laser cavity mode and phase lock.

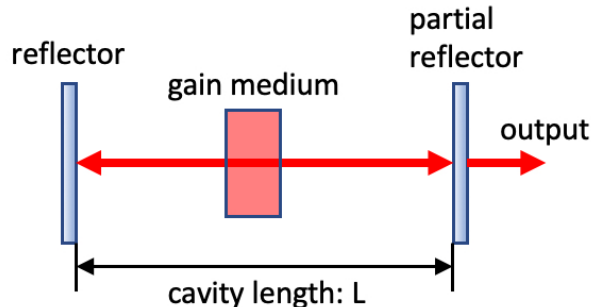


Figure 2.1: Schematic of a linear laser cavity

Figure 2.1 shows the schematic of a linear laser cavity. Gain medium keeps getting excited by pump source, providing gain for light amplification. Two reflectors form a resonator, with cavity length of L . Light is confined in the resonator and keeps getting amplified by the gain medium. Part of the light is coupled out of the cavity as laser output. Lasing can only happen if wavelength (frequency) of light satisfies standing wave condition of the resonator. These are called longitudinal modes of the laser cavity. Frequency spacing of adjacent longitudinal modes is expressed by

$$\Delta\omega = \pi c/L_c \quad (2.1)$$

where c is the speed of light in vacuum and L_c is the optical length of the cavity. Longitudinal modes that fall into the gain spectrum have the chance to oscillate. For a typical fiber laser with 10 m cavity length, there are around 10^5 longitudinal modes within gain

spectrum. For simplicity, assume that there are $N = 2M + 1$ longitudinal modes with the same amplitude and initial phase being phase locked, superposition of the electric field is expressed by

$$E(t) = \sum_{m=-M}^M E_0 \cos(\omega_0 t + \phi_0 + m\Delta\omega t) = E_0 \frac{\sin(2M+1)\Delta\omega t/2}{\sin\Delta\omega t/2} \cos(\omega_0 t + \phi_0) \quad (2.2)$$

where E_0 , ω_0 , ϕ_0 and $\Delta\omega$ are the amplitude of the longitudinal modes, frequency of the 0th longitudinal mode, initial phase of the longitudinal modes and frequency spacing of adjacent longitudinal modes. Thus, optical intensity of the electrical field envelop is expressed by

$$I(t) = \frac{\sin^2(2M+1)\Delta\omega t/2}{\sin^2\Delta\omega t/2} E_0^2 \quad (2.3)$$

Here, $I(t)$ exhibits as a short pulse with peak intensity of $N^2 E_0^2$ at $t = 0$.

2.2 Mode Locking Techniques

Mode locking methods can be classified into active mode locking and passive mode locking [19]. In active mode locking, an external modulation is usually applied to laser cavity [2, 20]. In passive mode locking, a saturable absorber (SA) is applied for generating optical pulse [12, 13, 15].

2.2.1 Active Mode Locking

Figure 2.2 shows the schematic of active mode locking by amplitude modulation. In conventional active mode locking by amplitude modulation, a loss modulator is inserted in the laser cavity. Loss modulation frequency of the cavity equals the round trip time of laser cavity, which is also the reciprocal of the longitudinal mode spacing. Thus, pulses can pass the loss modulator when it suffers the minimum loss, as shown in Figure 2.3.

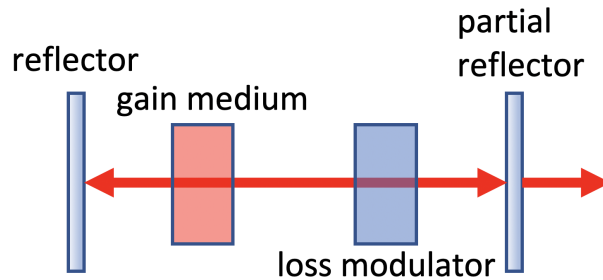


Figure 2.2: Schematic of active mode locking by amplitude modulation

Active mode locking can also be described in frequency domain, as shown in Figure 2.4. The figure shows seven longitudinal modes. When amplitude modulation is applied at the same frequency as longitudinal mode spacing, two side longitudinal modes with the same phase are generated in each side of the central longitudinal mode every round trip. After numbers of round trips, phase relation of all these longitudinal modes is fixed.

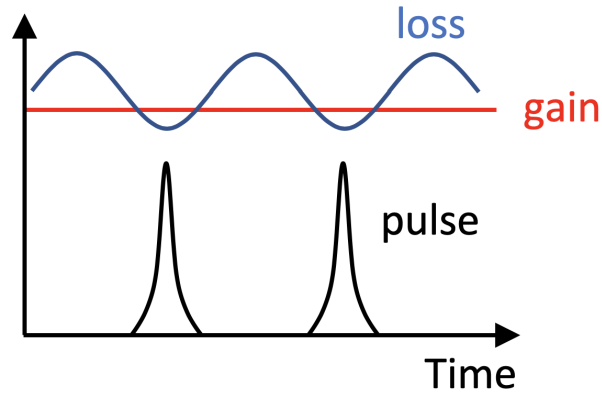


Figure 2.3: Active mode locking by amplitude modulation in time domain

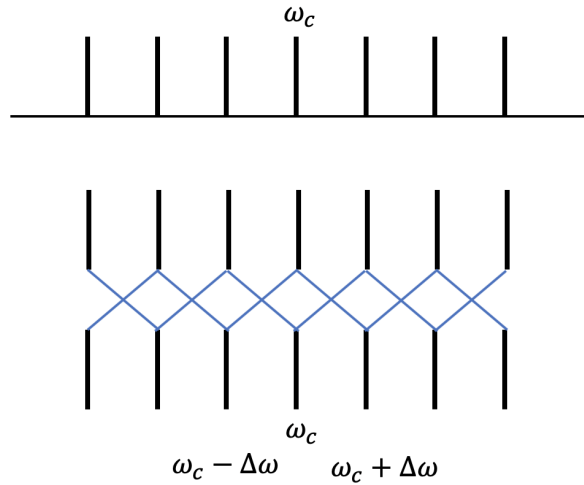


Figure 2.4: Active mode locking by amplitude modulation in frequency domain

In this thesis, we mainly focus on another novel active mode locking method: active mode locking via pump modulation (AMPM). Instead of modulating cavity loss, cavity gain is modulated by modulating pump power. Detailed concept and principle of AMPM will be shown in Chapter 4.

2.2.2 Passive Mode Locking

In passive mode locking method, a saturable absorber (SA) is applied in the laser cavity. The purpose of SA is similar to a modulator in active mode locking. SA typically shows lower transmission to low intensity light and higher transmission to higher intensity light. This property of SA can help narrow down pulse width effectively, as shown in Figure 2.5. After laser is started, pulses can be formed from laser noise by the self-modulation effect of SA. Figure 2.6 shows the schematic of passive mode locking. Next, we will introduce four types of commonly used SAs in fiber lasers.

Semiconductor saturable absorber mirror

Semiconductor saturable absorber mirror (SESAM) was invented by U. Keller and her

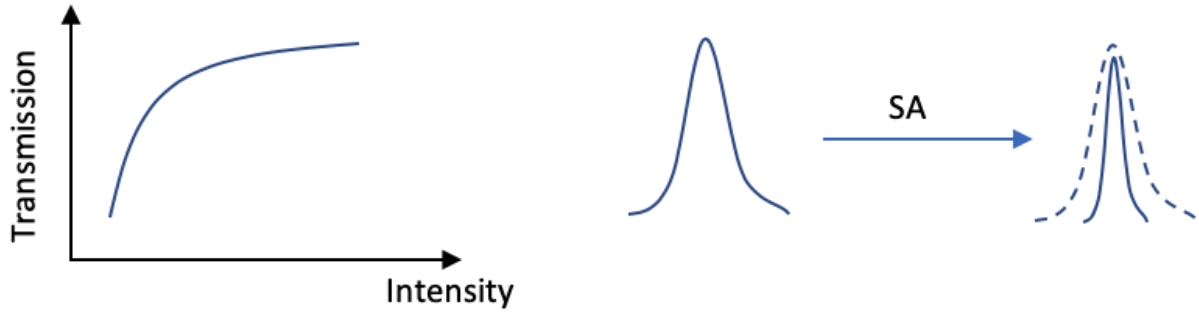


Figure 2.5: Saturable absorber

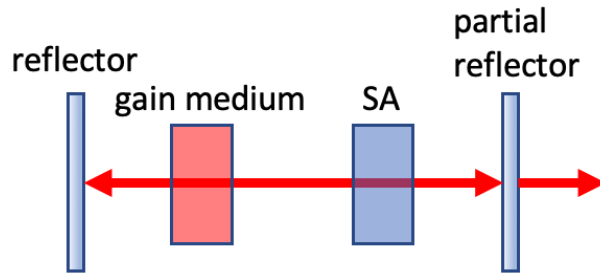


Figure 2.6: Schematic of passive mode locking

coworkers in 1992 [12]. A SESAM typically consists of a semiconductor Bragg mirror acting as a reflecting mirror and a quantum well absorber acting as a saturable absorber. Physical mechanism of its saturable absorption is as follows: when light is absorbed by SESAM, photon energy is transfer to electrons, which are brought from valence band to conduction band. At low incident intensity, photon absorption remains unsaturated, resulting a higher loss. At high intensity, photon absorption gets saturated. In this case, absorption does not increase as incident intensity increases, resulting a higher transmission at higher intensity.

Although SESAM was invented and mostly used for mode locking a solid-state laser, it can also be applied for fiber laser. SESAM are fabricated by semiconductor material deposition technique, making it convenient for controlling and tailoring, such as parameters like modulation depth and saturation fluence. These advantages make it one of the most widely applied SAs in commercial mode locked lasers.

Nonlinear polarization rotation

Nonlinear polarization rotation (NPR) refers to the intensity dependent change of polarization state due to self-phase modulation (SPM) and cross-phase modulation (XPM). Artificial saturable absorption can be led by incorporating NPR and polarization dependent loss (PDL) component. In mode locked fiber laser using NPR, a polarizer and two polarization controllers (PCs) are usually applied. PCs are used to control the polarization state of light in laser cavity, forcing the light with high intensity to pass the polarizer with higher transmission and low intensity light with low transmission. Figure 2.7 shows a typical setup for NPR mode locked fiber laser.

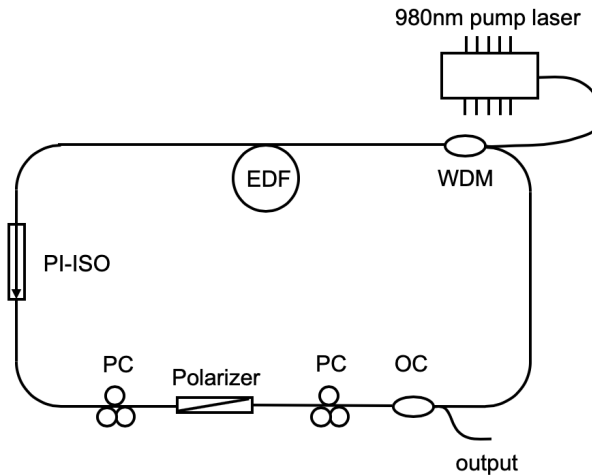


Figure 2.7: Typical schematic of NPR mode locked fiber laser

Nonlinear amplifying loop mirror

Nonlinear amplifying loop mirror (NALM) can also function as an artificial saturable absorber [21]. Schematic of nonlinear amplifying loop mirror is shown in Figure 2.8. Input light is split into clockwise and counter-clockwise direction by a 50:50 coupler. When there is no gain fiber in the fiber loop, the fiber loop is symmetrical. In this case, clockwise and counter-clockwise light will interfere at coupler. The combined light will be totally reflected back to input port. When gain fiber is inserted as in Figure 2.8, the fiber loop becomes asymmetrical. Counter-clockwise light will be firstly amplified and propagate through relatively long passive fiber. However, for clockwise light, it will firstly propagate through passive fiber and then be amplified. Consequently, light will suffer different amount of nonlinear phase shift between counter-clockwise and clockwise direction. When they interfere at the coupler, part of the combined light is reflected back to the input port, while the other part goes to the output port. Therefore, the transmission (reflection) of the fiber loop becomes intensity dependent. Figure 2.9 shows a typical schematic of NALM mode locked fiber laser, also known as "figure-8 laser".

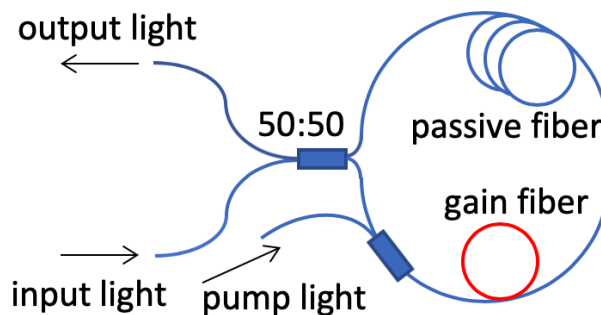


Figure 2.8: Schematic of nonlinear amplifying loop mirror

Carbon nanotube

Carbon nanotube (CNT) is a type of nanomaterial consisting of a two dimensional hexag-

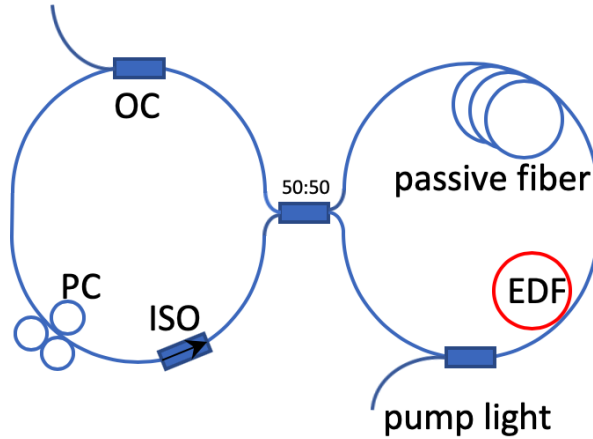


Figure 2.9: Typical schematic of NALM mode locked fiber laser

onal lattice of carbon atoms, as shown in Figure 2.10 [15, 22]. The physical mechanism of CNT saturable absorber is similar to that of SESAM. Photon absorption of CNT remains unsaturated at low intensity. At high intensity, CNT gets saturated, resulting a higher transmission.



Figure 2.10: Carbon nanotube [22]

2.3 Pulse Propagation in Optical Fiber

Optical pulse propagation in optical fiber is described by the following equation:

$$\frac{\partial A}{\partial z} + \frac{i\beta_2}{2} \frac{\partial^2 A}{\partial T^2} + \frac{\alpha}{2} A = i\gamma |A|^2 A \quad (2.4)$$

where A is the slowly varying envelop of the pulse electric field, as a function of propagation length along the fiber z and time T . β_2 is second order chromatic dispersion of fiber,

also known as group velocity dispersion (GVD). α is fiber loss and γ is fiber nonlinearity. Detailed derivation of Eq. (2.4) is shown in Appendix. In gain fiber, Eq. (2.4) becomes:

$$\frac{\partial A}{\partial z} + \frac{i\beta_2}{2} \frac{\partial^2 A}{\partial T^2} + \frac{\alpha - g}{2} A = i\gamma|A|^2 A \quad (2.5)$$

where g is fiber gain.

Next, we will introduce each parameter in more detail.

Chromatic dispersion

Chromatic dispersion comes from the frequency dependence of refractive index $n(\omega)$. It results different speed of light for different frequency components in optical fiber. To analyze the effects of chromatic dispersion, we expand mode-propagation constant β in Taylor series about the frequency:

$$\beta(\omega) = n(\omega) \frac{\omega}{c} = \beta_0 + \beta_1(\omega - \omega_0) + \frac{1}{2}\beta_2(\omega - \omega_0)^2 + \dots \quad (2.6)$$

where

$$\beta_m = \left(\frac{d^m \beta}{d\omega^m} \right)_{\omega=\omega_0} \quad (m = 0, 1, 2, \dots) \quad (2.7)$$

Here we focus on first-order and second-order.

$$\beta_1 = \frac{d\beta}{d\omega} = \frac{1}{c} \left(n + \omega \frac{dn}{d\omega} \right) = \frac{1}{v_g} \quad (2.8)$$

$$\beta_2 = \frac{d^2\beta}{d\omega^2} = \frac{d}{d\omega} \left(\frac{1}{v_g} \right) \quad (2.9)$$

where v_g is group velocity. β_1 represents the optical pulse propagation speed along the fiber and β_2 represents the group velocity dispersion, responsible for pulse broadening and compression. Dispersion parameter D is often used to represent GVD, defined as:

$$D = \frac{d\beta_1}{d\lambda} \quad (2.10)$$

It is related to β_2 as:

$$D = \frac{d\beta_1}{d\lambda} = -\frac{2\pi c}{\lambda^2} \beta_2 \quad (2.11)$$

Figure 2.11 shows the dispersion parameter D with wavelength for a single-mode fiber [23]. GVD becomes zero at wavelength around $1.3 \mu m$. This wavelength is called zero-dispersion wavelength. GVD has different sign at different side of zero-dispersion wavelength. At shorter wavelength, $D < 0$ and $\beta_2 > 0$. Fiber exhibits normal dispersion. High frequency components travel slower than low frequency components at normal dispersion. At longer wavelength, $D > 0$ and $\beta_2 < 0$. Fiber exhibits anomalous dispersion. High frequency components travel faster than low frequency components at anomalous dispersion. GVD is one of the most important parameters for mode locked fiber laser. Specially, fiber nonlinearity and anomalous dispersion can cancel each other and support soliton to help mode locking. More detailed analysis of effects of normal dispersion and anomalous dispersion on mode locking will be explained in Chapter 4, Section 4.4.

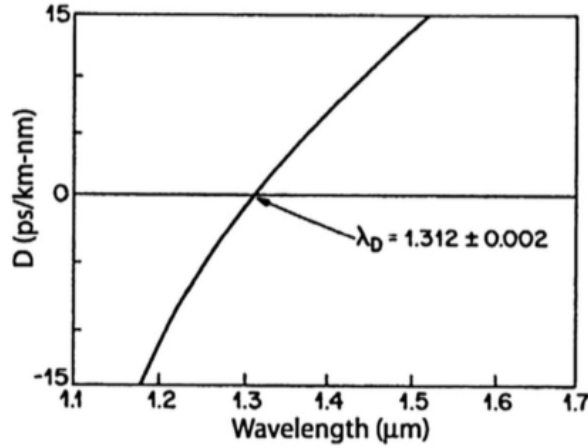


Figure 2.11: Dispersion parameter with wavelength for a single-mode fiber [23]

Fiber loss

Fiber loss is an important parameter for optical fiber, defined as follows:

$$P_T = P_0 \exp(-\alpha L) \quad (2.12)$$

where P_0 is the input power and P_T is the transmitted power after fiber length L . Fiber loss is also commonly expressed in decibel unit:

$$\alpha_{dB} = -\frac{10}{L} \log \left(\frac{P_T}{P_0} \right) \simeq 4.343\alpha \quad (2.13)$$

Loss of standard silica fiber used for telecommunication is wavelength dependent, as shown in Figure 2.12. Fiber exhibits a minimum loss of around 0.2 dB/km near $1.55 \mu\text{m}$, making $1.55 \mu\text{m}$ the window for fiber-optic telecommunications. Fiber loss is mainly from Rayleigh scattering and material absorption. Dashed curve in Figure 2.12 shows the loss resulted from Rayleigh scattering. The peak near $1.4 \mu\text{m}$ is led by OH-ion absorption.

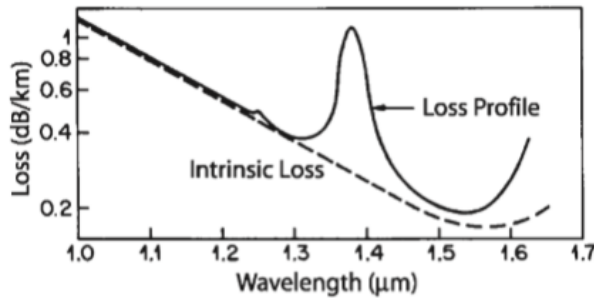


Figure 2.12: Fiber loss with wavelength. Dashed curve shows the loss resulted from Rayleigh scattering [23].

Fiber gain

Parameter g stands for amplification of gain fiber. Amplification of gain fiber is dependent

on the input signal power. Here, g can be modeled as:

$$g = \frac{g_s}{1 + E_p/E_s} \quad (2.14)$$

where g_s is the small signal gain of the gain fiber and E_s is the saturation energy of the gain fiber, which is related to the pumping level. E_p is pulse energy and can be calculated by:

$$E_p = \int_{-\infty}^{\infty} |A|^2 dT \quad (2.15)$$

In some cases, the wavelength dependency of g must be considered. Then we rewrite g as:

$$g = \frac{g_s}{1 + E_p/E_s} g(\omega) \quad (2.16)$$

where $g(\omega)$ describes the wavelength dependency of g and has no unit.

Fiber nonlinearity

Fiber nonlinearity refers to the phenomenon that the response of optical fiber becomes nonlinear at high intensity. The nonlinearity of optical fiber originated from the induced nonlinear electric polarization. Total induced polarization \mathbf{P} is related to electric field \mathbf{E} by the following equation:

$$\mathbf{P} = \epsilon_0 \left(\chi^{(1)} \cdot \mathbf{E} + \chi^{(2)} : \mathbf{E}\mathbf{E} + \chi^{(3)} : \mathbf{E}\mathbf{E}\mathbf{E} + \dots \right) \quad (2.17)$$

where ϵ_0 is the vacuum permittivity and $\chi^{(j)}$ is the j th-order susceptibility. Since silica is a symmetric molecule, $\chi^{(2)} = 0$. Therefore the third-order susceptibility $\chi^{(3)}$ causes the lowest-order nonlinearity, which is responsible for nonlinear refraction.

In the simplest case, nonlinear refractive index can be expressed as:

$$\tilde{n}(\omega, I) = n(\omega) + n_2 I = n + \tilde{n}_2 |E|^2 \quad (2.18)$$

where $n(\omega)$ is the linear part, E is the electric field, and \tilde{n}_2 is the nonlinear-index coefficient

$$\tilde{n}_2 = \frac{3}{8n} \Re(\chi_{xxxx}^{(3)}) \quad (2.19)$$

where $\Re(\chi_{xxxx}^{(3)})$ stands for the real part of $\chi_{xxxx}^{(3)}$.

Nonlinear refraction index leads to some interesting nonlinear effects, such as self-phase modulation (SPM) and cross-phase modulation (XPM). Here we pay special attention to SPM, which refers to the phase modulation induced by the pulse itself as it propagates along the fiber. Phase change can be written as:

$$\phi = \tilde{n} k_0 L = (n + \tilde{n}_2 |E|^2) k_0 L \quad (2.20)$$

where $k_0 = 2\pi/\lambda$ and L is the fiber length. Here, $\phi_{NL} = \tilde{n}_2 k_0 L |E|^2$ is the nonlinear phase change induced by SPM. SPM is responsible for spectral broadening and soliton formation at anomalous dispersion regime. In Eq (2.4), γ stands for SPM.

2.4 Pulse Shaping at Anomalous Dispersion and Normal Dispersion

As has been introduced in the last section, pulse will experience the effects of loss, gain (with gain dispersion), nonlinearity and dispersion in optical fiber. Plus, in a mode locked fiber laser, a modulator (in active mode locking) or SA (in passive mode locking) is needed, which will lead to the effect amplitude modulation on the pulse itself. In some cases, spectral filtering effect is also important to pulse shaping. To put these together, we usually consider the effects of loss/gain, amplitude modulation (modulator or SA), phase modulation (nonlinearity), dispersion and spectral filtering in a mode locked fiber laser.

At anomalous dispersion ($\beta_2 < 0$), such as Er-doped fiber laser and Tm-doped fiber laser, soliton pulse is usually formed. In this case, only nonlinearity and anomalous dispersion are determinant in shaping the pulse. Effects of fiber nonlinearity and dispersion cancel each other, resulting a stationary pulse traveling along the cavity.

However at normal dispersion ($\beta_2 > 0$), only nonlinearity and dispersion can not balance each other. One way to help mode locking is to compensate the dispersion. When normal dispersion and anomalous dispersion are of equal importance to the pulse shaping, stretched pulse (dispersion managed soliton) can be formed [24]. Pulse shaping at all normal dispersion is also possible [25]. Strong amplitude modulation is determinant for all normal dispersion pulse shaping.

2.5 Simulation Method

Eq. (2.4) is a nonlinear partial differential equation which can usually not be solved analytically. Therefore it is necessary for a numerical simulation method to solve this equation. This section will introduce one of the most widely applied method: split-step Fourier method.

Firstly, we write Eq (2.4) in the following form:

$$\frac{\partial A}{\partial z} = (\widehat{D} + \widehat{N})A \quad (2.21)$$

where \widehat{D} is a linear differential operator for dispersion and fiber losses, \widehat{N} is a nonlinear operator for fiber nonlinearity. They are given by:

$$\widehat{D} = -\frac{i\beta_2}{2} \frac{\partial^2}{\partial T^2} - \frac{\alpha}{2} \quad (2.22)$$

$$\widehat{N} = i\gamma|A|^2 \quad (2.23)$$

In split-step Fourier method, we regard dispersion and nonlinearity act separately over a small distance. To be specific, in the propagation from z to $z + h$, $A(z + h, T)$ can be calculated as:

$$A(z + h) \approx \exp(h\widehat{D}) \exp(h\widehat{N})A(z, T) \quad (2.24)$$

Here, $\exp(h\hat{D})$ can be evaluated in Fourier domain by:

$$\exp(h\hat{D})B(z, T) = F_T^{-1} \exp[h\hat{D}(-i\omega)]F_TB(z, T) \quad (2.25)$$

where F_T and F_T^{-1} stands for Fourier tranform and inverse Fourier transform respectively. Fourier transform can be implemented by FFT algorithm, making split-step Fourier transform method a rather fast numerical method for simulating pulse propagation in optical fibers. $\hat{D}(-i\omega)$ is obtained by replacing $\partial/\partial T$ with $-i\omega$ in Eq. (2.22).

Eq. (2.5) can be solved numerically in the same way as Eq. (2.4). An example for simulating Eq. (2.5) in MATLAB is shown in Appendix.

Chapter 3

Pump to Signal Transfer of Modulation Index in Gain Fiber

In the technique of active mode locking via pump modulation (AMPM), cavity gain is modulated by modulating the pump power. Therefore it is important to understand how pump modulation is transferred to signal in gain fiber. In this chapter, we will firstly show the analytical model for pump modulation in gain fiber. Then, we will present our experimental measurement results on ytterbium-doped, thulium-doped and erbium-doped fiber. Experimental results show the low-pass filtering characteristics of pump to signal transfer of modulation index, which matches well with the theory model.

3.1 Theoretical Model of Gain Modulation

Gain modulation was studied in investigated in Er-doped fiber amplifier systems for optical fiber telecommunications [26–28]. Especially, an analytical model for pump modulation was systematically studied in Ref [29]. Pump modulation is considered as a perturbation of the steady-state. Firstly, we consider the steady-state of excited ion density. Three-level system is adopted for gain fiber, as shown in Figure 3.1. n_1 is the ground state ion density. n_2 is the excited state ion density related to signal. n_3 is the excited state ion density related to pump. Rate equations for describing this three-level system are given by:

$$\begin{cases} \frac{\partial}{\partial t}n_1 = -R_{13}n_1 - W_{12}n_1 + W_{21}n_2 + \frac{n_2}{\tau} + R_{31}n_3 + \frac{n_3}{\tau'} \\ \frac{\partial}{\partial t}n_2 = W_{12}n_1 - W_{21}n_2 + R_{32}n_3 - \frac{n_2}{\tau} \\ \frac{\partial}{\partial t}n_3 = R_{13}n_1 - R_{32}n_3 - R_{31}n_3 - \frac{n_3}{\tau'} \end{cases} \quad (3.1)$$

where W is responsible for transition related to signal and R is responsible for transition related to pump.

In practice, $R_{32} \gg R_{31}$ and $R_{32} \gg 1/\tau'$. Therefore at steady state, $R_{13}n_1 = R_{32}n_3$. If we assume $R_{32} \gg R_{13}$, $N_3 \approx 0$ and Eq. (3.1) becomes:

$$\frac{\partial}{\partial t}n_2 = W_{12}n_1 - W_{21}n_2 + R_{13}n_1 - \frac{n_2}{\tau} \quad (3.2)$$

Since $N_3 \approx 0$, we have $n_1 + n_2 = \rho$, where ρ is the ion density. The transition rate W_{12} , W_{21} and R_{13} are proportional to the pump or signal power, shown as follows:

$$W_{12} = \frac{\Gamma_S \sigma_{12} P_S}{A} \quad (3.3)$$

$$W_{21} = \frac{\Gamma_S \sigma_{21} P_S}{A} \quad (3.4)$$

$$R_{13} = \frac{\Gamma_P \sigma_{13} P_P}{A} \quad (3.5)$$

where P_P and P_S are pump power and signal power, in photons per second. A is the effective cross-sectional area of fiber core. σ_{12} , σ_{13} and σ_{21} are the cross section data of signal absorption, pump absorption and signal emission. Γ_S and Γ_P are the mode confinement factors for signal and pump wave in fiber.

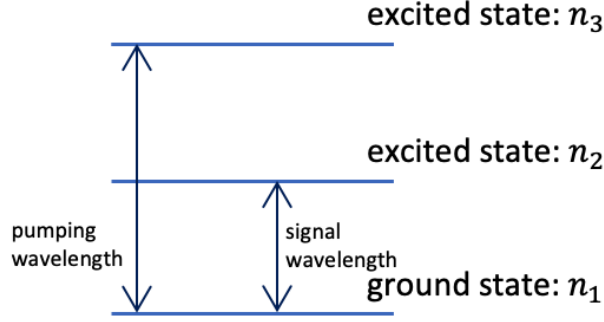


Figure 3.1: Three-level system

As pump and signal propagate along the gain fiber, pump gets absorbed and signal gets amplified. They are determined by the following equations:

$$\frac{\partial}{\partial z} P_P = -\Gamma_P \sigma_{13} n_1 P_P - \gamma_P P_P \quad (3.6)$$

$$\frac{\partial}{\partial z} P_S = -\Gamma_S \sigma_{12} n_1 P_S + \Gamma_S \sigma_{21} n_2 P_S - \gamma_S P_S \quad (3.7)$$

Here, γ is responsible for scattering and losses of gain fiber and can usually be neglected. By substituting Eqs. (3.3) through (3.5) into Eqs. (3.6) and (3.7) and neglecting γ s, we have:

$$\frac{\partial}{\partial z} P_P = -R_{13} A n_1 \quad (3.8)$$

$$\frac{\partial}{\partial z} P_S = -W_{12} A n_1 + W_{21} A n_2 \quad (3.9)$$

Multiplying Eq. (3.2) by A and substituting Eqs. (3.8) and (3.9) into Eq. (3.2), we have:

$$\frac{\partial}{\partial z} (n_2 A) = -\frac{\partial}{\partial z} P_S - \frac{\partial}{\partial z} P_P - \frac{n_2 A}{\tau} \quad (3.10)$$

Integrating (3.10) over z , we have:

$$\frac{\partial}{\partial t} N_2 = P_S(0, t) - P_S(L, t) + P_P(0, t) - P_P(L, t) - \frac{N_2}{\tau} \quad (3.11)$$

where N_2 is the total number of excited ions in gain fiber from 0 to L . $P_S(0, t)$ and $P_P(0, t)$ are the signal and pump power at the start of gain fiber. $P_S(L, t)$ and $P_P(L, t)$ are the signal and pump power at the end of gain fiber. From Eqs. (3.6) and (3.7), we have:

$$\frac{P_P(L, t)}{P_P(0, t)} = \exp\left(-\frac{\Gamma_P \sigma_{13} N_1}{A}\right) \quad (3.12)$$

$$\frac{P_P(L, t)}{P_P(0, t)} = \exp\left(-\frac{\Gamma_S \sigma_{12} N_1}{A} + \frac{\Gamma_S \sigma_{21} N_2}{A}\right) \quad (3.13)$$

By $N_1 = \rho LA - N_2$, Eqs. (3.12) and (3.13) can be simplified as:

$$\frac{P_P(L, t)}{P_P(0, t)} = \exp(B_P N_2 - C_P) \quad (3.14)$$

$$\frac{P_S(L, t)}{P_S(0, t)} = \exp(B_S N_2 - C_S) \quad (3.15)$$

where

$$B_P = \frac{\Gamma_P \sigma_{13}}{A} \quad (3.16)$$

$$B_S = \Gamma_S \frac{\sigma_{12} + \sigma_{21}}{A} \quad (3.17)$$

$$C_P = \Gamma_P \sigma_{13} \rho L \quad (3.18)$$

$$C_S = \Gamma_S \sigma_{12} \rho L \quad (3.19)$$

Eqs. (3.14) and (3.15) show the relation between $P_P(L, t)$ and $P_P(0, t)$, and also the relation between $P_S(L, t)$ and $P_S(0, t)$. By using this relation, we can simplify Eq. (3.11) as:

$$\frac{\partial}{\partial t} N_2 = P_S(0, t)[1 - \exp(B_S N_2 - C_S)] + P_P(0, t)[1 - \exp(B_P N_2 - C_P)] - \frac{N_2}{\tau} \quad (3.20)$$

Pump modulation is considered as a perturbation of the steady-state. In this case, we solve for the steady-state solution of Eq. (3.20) first. We consider its expansion about its steady-state solution:

$$N_2(t) = N_2^0(1 + \delta \cos(\omega t + \phi)) \quad (3.21)$$

where N_2^0 is the steady state solution. δ and φ are to be determined. By substituting Eq. (3.21) and $\partial N_2^0 / \partial t = 0$ into Eq. (3.20), we have:

$$0 = P_S^0(0)[1 - \exp(B_S N_2^0 - C_S)] + P_P^0(0)[1 - \exp(B_P N_2^0 - C_P)] - \frac{N_2^0}{\tau} \quad (3.22)$$

where $P_S^0(0)$ and $P_P^0(0)$ are mean signal and pump power at $z = 0$. Approximate solution of Eq. (3.22) can be solved by taking the first-order terms in the expansion of the exponential, given as:

$$N_2^0 \approx \frac{C_P P_P^0(0) + C_S P_S^0(0)}{B_P P_P^0(0) + B_S P_S^0(0) + \frac{1}{\tau}} \quad (3.23)$$

Next we consider the pump modulation as perturbation. Assume the input pump power is:

$$P_P^0(0, t) = P_P^0(0)(1 + m_P \cos \omega t) \quad (3.24)$$

where m_P is the modulation index and ω is the modulation frequency. By substituting Eqs. (3.21) and (3.24) into Eq. (3.20), we have:

$$\begin{aligned} -N_2^0 \delta \omega \sin(\omega t + \phi) = & P_S^0(0) [1 - \exp(B_S N_2^0 \times (1 + \delta \cos(\omega t + \phi)) - C_S)] \\ & + P_P^0(0) (1 + m_P \cos \omega t) \times [1 - \exp(B_P N_2^0 \\ & \times (1 + \delta \cos(\omega t + \phi)) - C_P)] - N_2^0 \frac{1 + \delta \cos(\omega t + \phi)}{\tau} \end{aligned} \quad (3.25)$$

By taking the first-order approximation of δ , we can solve for ϕ and δ , given by:

$$\tan \phi = -\frac{\omega}{\omega_{eff}} \quad (3.26)$$

$$\delta = \frac{m_P [P_P^0(0) - P_P^0(L)]}{N_2^0 \sqrt{\omega^2 + \omega_{eff}^2}} \quad (3.27)$$

where $\omega_{eff} = P_S^0(L)B_S + P_P^0(L)B_P + 1/\tau$. Then, we get the modulated signal by using Eq. (3.15):

$$\begin{aligned} P_S(L, t) = & P_S^0(0) \exp \{ B_S N_2^0 (1 + \delta \cos(\omega t + \phi)) - C_S \} \\ \approx & P_S^0(L) (1 + B_S N_2^0 \delta \cos(\omega t + \phi)) \end{aligned} \quad (3.28)$$

Here, we took small modulation approximation at " \approx " sign. Specifically, modulation index transfer function can be written as:

$$H_{P \rightarrow S} = \frac{m_S}{m_P} = \frac{B_S [P_P^0(0) - P_P^0(L)]}{\sqrt{\omega^2 + \omega_{eff}^2}} \quad (3.29)$$

This equation shows the low-pass filter characteristics of pump to signal transfer in gain fiber, with a cutoff wavelength of ω_{eff} .

3.2 Experimental Measurement of Pump to Signal Transfer

Last section showed the theoretical model of pump to signal transfer in gain fiber. In this section, we will conduct experimental measurements on pump to signal transfer of modulation index in Yb, Tm and Er-doped fiber.

Measurement on the Yb-doped fiber

Figure 3.2 shows the schematic of our measurement system. 980 nm pump light directly comes from a laser diode (LD) modulated by signal generator with sinusoidal waveform. WDM2 couples pump light into the Yb-doped fiber and residual pump is coupled out of the system by WDM1. Yb-doped fiber used in the measurement is 0.3 m. Here, we employed backward pumping so that residual pump would not interfere with our measurement.

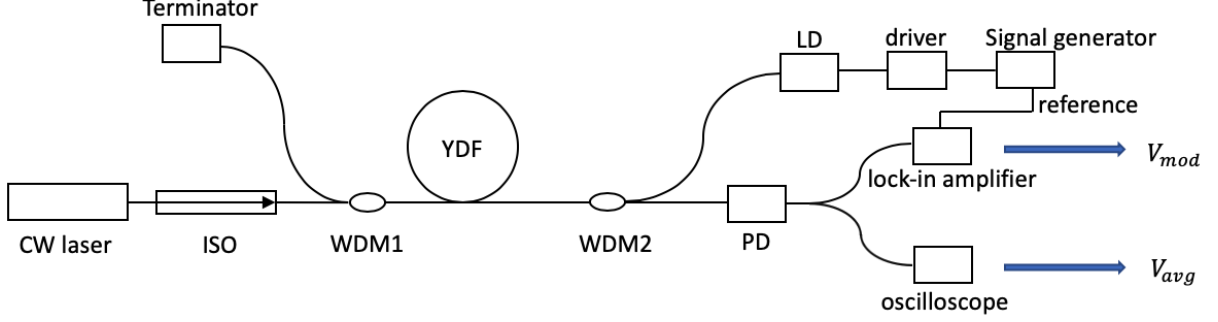


Figure 3.2: Experimental setup for measuring pump to signal transfer T in Yb-doped fiber

Assuming the input pump power P_P and modulated output signal P_S are described by:

$$P_P = P_P^0(1 + m_P \cos \omega t) \quad (3.30)$$

$$P_S = P_S^0(1 + m_S \cos(\omega t + \phi)) \quad (3.31)$$

where P_P^0 and P_S^0 are average values. m_P and m_S are modulation indexes. ω is the modulation frequency and ϕ is the phase difference between signal and pump modulation. Pump to signal transfer of modulation index is given as:

$$T = \frac{m_S}{m_P} \quad (3.32)$$

which is to be measured by the system. CW source has an operation wavelength of 1.03 μm , providing the seed signal to be amplified. Amplified optical signal is received by a photodetector (PD, Model: DET08CFC/M, 5 GHz, from THORLABS) and transformed into electrical signal, which splits into two and measured with a lock-in amplifier and an oscilloscope respectively. Modulated signal power and average power are measured to be V_{mod} and V_{avg} . Thus, modulation index of signal m_S can be calculated by:

$$m_S = CV_{mod}/V_{avg} \quad (3.33)$$

where C is the calibration coefficient between the lock-in amplifier and oscilloscope.

Since laser operates at saturated gain, we firstly measured the transfer at different saturation level, shown as dotted lines in Figure 3.3. The inset figure showed the saturation curve of the Yb-doped fiber at pump power of 67.9 mW and around 15% modulation index. Signal input power and gain are listed in Table 3.1. Cutoff frequency for A, B and C are 850 Hz, 1400 Hz and 3000 Hz respectively. Result shows that lower saturation leads to higher transfer at low frequency, but lower cutoff frequency at the same time. Solid

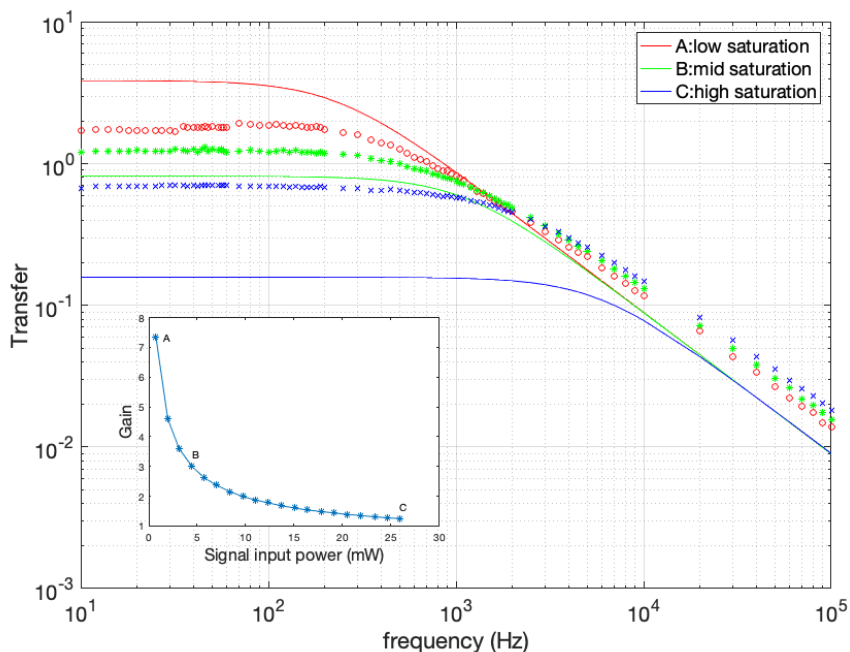


Figure 3.3: Transfer T at different saturation level in Yb-doped fiber. Dotted line: experimental measurements; solid line: simulations; inset: gain saturation.

Table 3.1: Measured saturation level in inset of Figure 3.3

Point	Input power (mW)	Gain (P_{out}/P_{in})
A	0.74	7.33
B	4.45	3
C	25.91	1.26

lines in Figure 3.3 are the simulation results using the theoretical model presented in the previous section.

We also measured the transfer at different pumping level, shown as dotted lines in Figure 3.4. Signal input power was set as $2 mW$, pump power are $45 mW$, $68 mW$ and $81 mW$ respectively. Results show that higher pump power leads to higher transfer. Solid lines are simulation results.

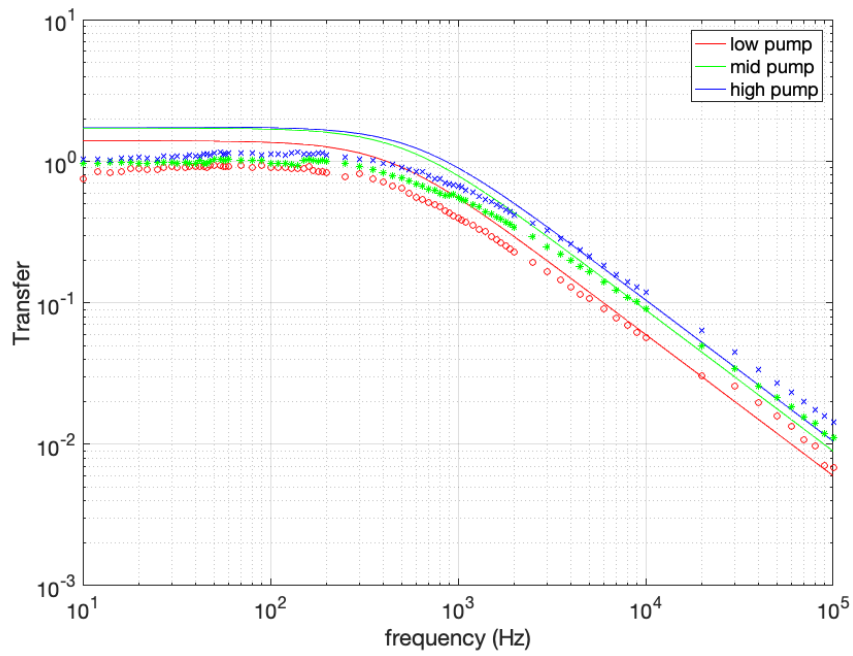


Figure 3.4: Transfer T at different pumping level in Yb-doped fiber. Dotted line: experimental measurements; solid line: simulations.

Measurement on the Tm-doped fiber

Measurement on Tm-doped fiber is similar to that of Yb-doped fiber. Measurement setup was shown in Figure 3.5. A 1570 nm CW source is amplified by an Erbium-doped fiber amplifier (EDFA) and then modulated by an acousto-optic modulator (AOM) with sinusoidal waveform. Tm-doped fiber (Model: TmDF200, from OFS) is 0.5 m. PD (Model: ET-5000F, from EOT) has a bandwidth of 12.5 GHz.

Transfer at different saturation level and pumping level were measured, shown in Figure 3.6 and 3.7. In Figure 3.6, pump power was 92 mW and the modulation index was 10%. Signal input power and gain are listed in Table 3.2. The transfer characteristics were similar to that of Yb-doped fiber, with cutoff frequency around 1 kHz.

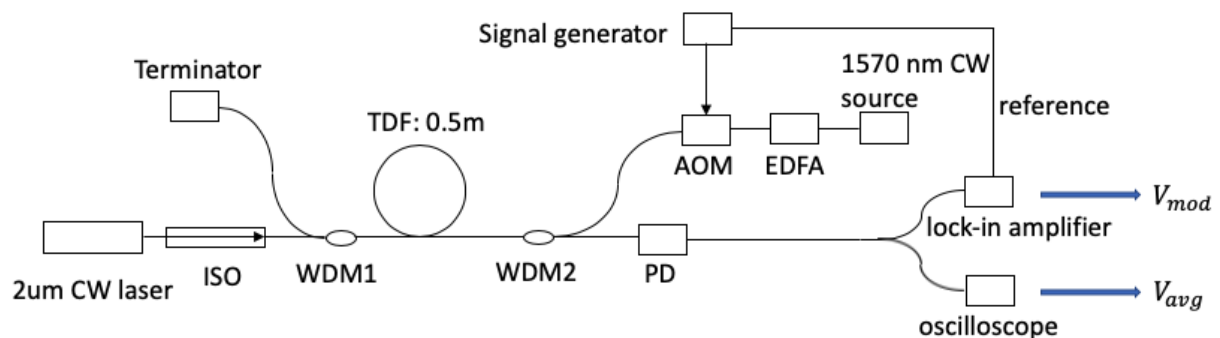


Figure 3.5: Experimental setup for measuring pump to signal transfer T in Tm-doped fiber

Table 3.2: Measured saturation level in inset of Figure 3.6

Point	Input power (mW)	Gain (P_{out}/P_{in})
A	0.16	3.25
B	8.98	1.52
C	1.77	2.39

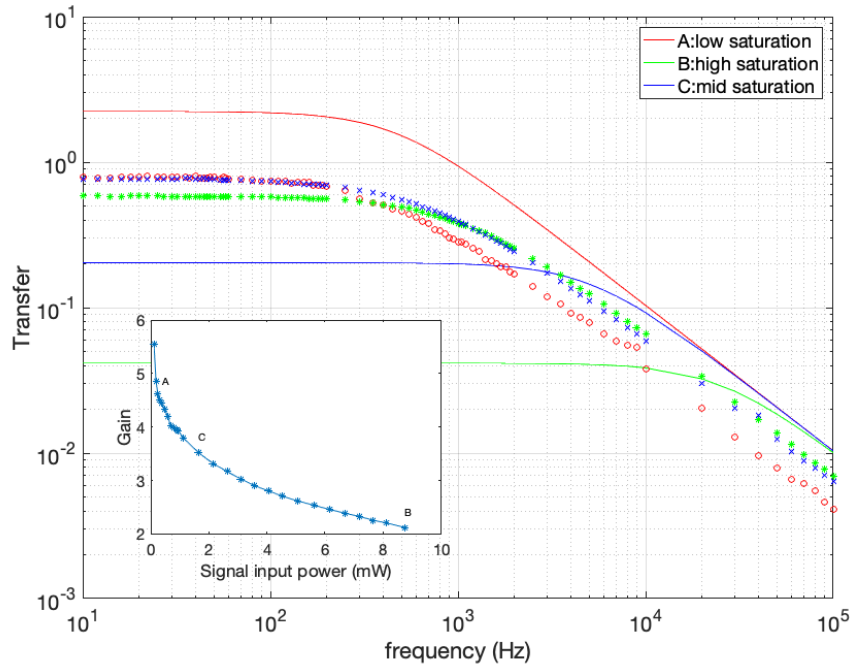


Figure 3.6: Transfer T at different saturation level in Tm-doped fiber. Dotted line: experimental measurements; solid line: simulations, inset: gain saturation.

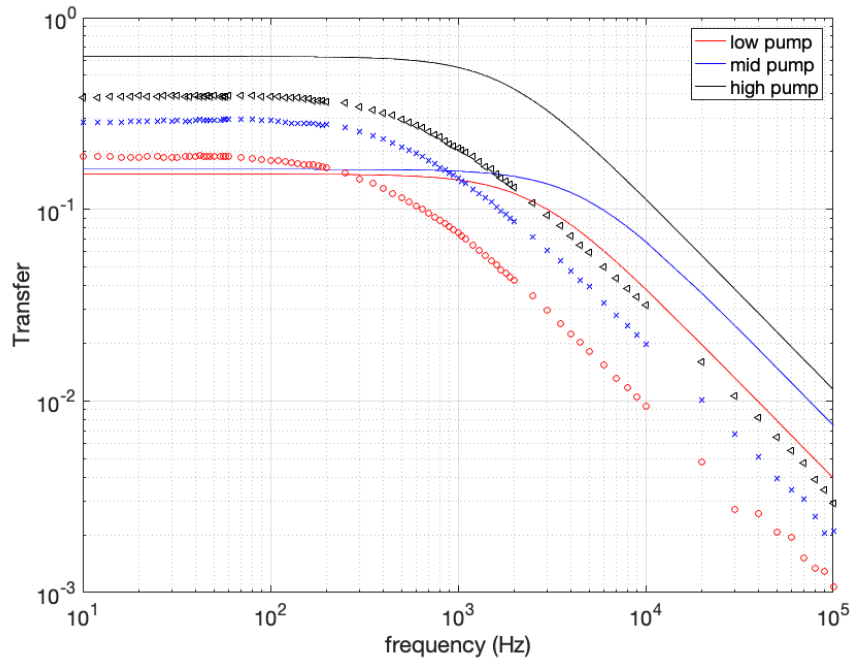


Figure 3.7: Transfer T at different pumping level in Tm-doped fiber. Dotted line: experimental measurements; solid line: simulations.

Measurement on the Er-doped fiber

Measurement on Er-doped fiber was also measured. Measurement setup was shown in Figure 3.8. Length of Er-doped fiber was 2 m (M-12-980-125, from THORLABS). PD has a bandwidth of 5 GHz (DET08CFC/M, from THORLABS).

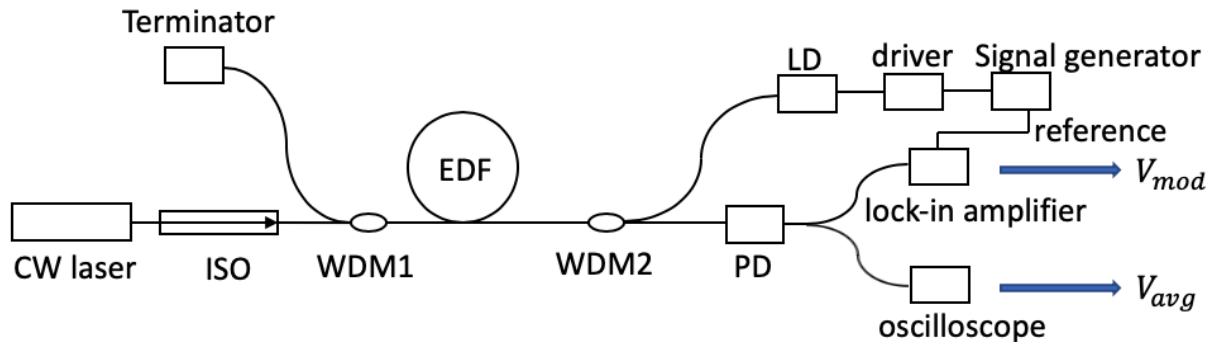


Figure 3.8: Experimental setup for measuring pump to signal transfer T in Er-doped fiber

Transfer at different saturation level and pumping level were measured, shown in Figure 3.9 and 3.10. In Figure 3.9, pump power was 84.8 mW and the modulation index was 15%. Signal input power and gain are listed in Table 3.3. In Figure 3.10, pump power are 129 mW, 84.8 mW and 39 mW, respectively. Cutoff frequency is around 700 Hz. Different from Tm and Yb-doped fiber, higher saturation leads to higher transfer while higher pump leads to lower transfer in Er-doped fiber.

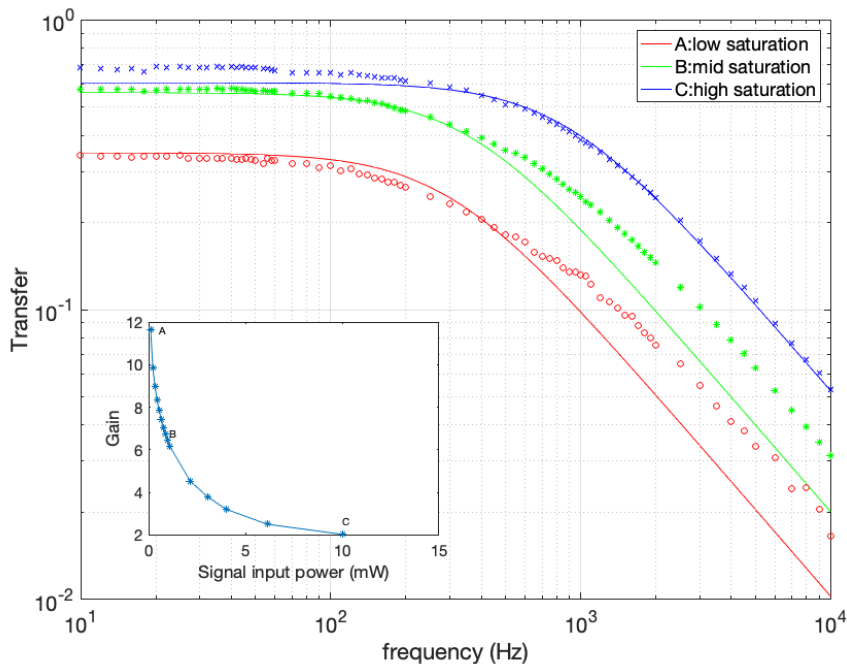


Figure 3.9: Transfer T at different saturation level in Er-doped fiber. Dotted line: experimental measurements; solid line: simulations, inset: gain saturation.

Table 3.3: Measured saturation level in inset of Figure 3.9

Point	Input power (mW)	Gain (P_{out}/P_{in})
A	0.109	11.6
B	1.09	6.19
C	10.01	2.04

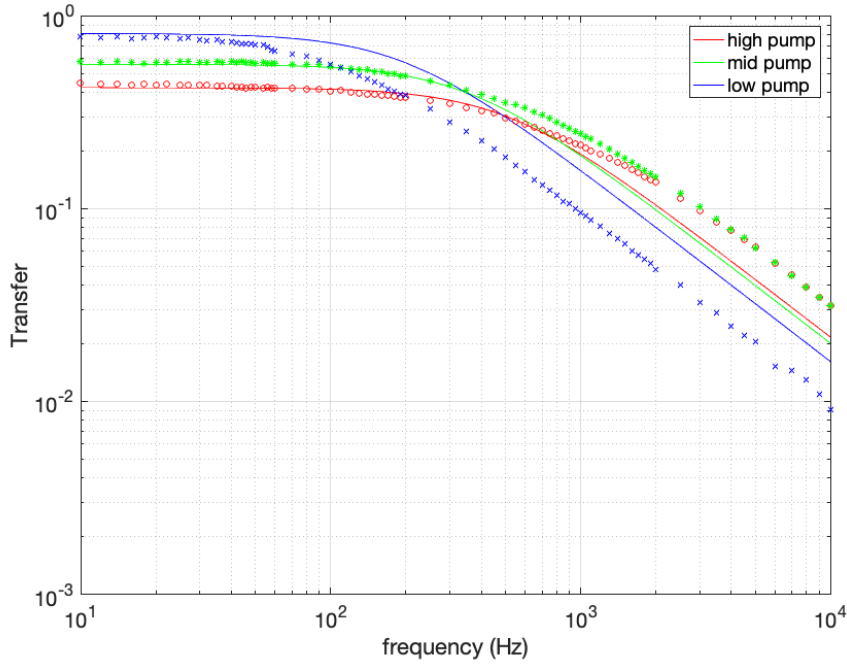


Figure 3.10: Transfer T at different pumping level in Er-doped fiber. Dotted line: experimental measurements; solid line: simulations.

3.3 Conclusion

In this chapter, we presented both theoretical model and experiment measurements on pump to signal transfer of modulation index in gain fiber. Theoretical model shows that the transfer exhibits a low-pass filter characteristics, whose cutoff frequency is related to ion upper-state lifetime.

Experiment measurement results confirmed the low-pass filter characteristics. Results showed that cutoff frequency of Yb and Tm-doped fiber were around 1-3 kHz while Er-doped fiber was around 700 Hz. Transfer at different saturation level and pumping level were also measured. For Yb and Tm-doped fiber, higher saturation led to lower transfer at low frequency while higher pump led to higher transfer. However, Er-doped fiber showed the opposite result: higher saturation led to higher transfer while higher pump led to lower transfer at low frequency.

IN GAIN

Chapter 4

Active Mode Locking via Pump Modulation

4.1 Introduction

Concept of mode locking has been introduced in Chapter 2, here we move to the main study of this thesis: ytterbium-doped mode locked fiber laser via pump modulation. Pump modulation is one type of active mode locking method, as shown in Figure 4.1. For conventional active mode locking, an external modulator is necessary, such as AOM [20] or lithium niobate modulator. However there are drawbacks of these modulators. For example, modulation frequency of AOM are usually limited. Although lithium niobate modulator is capable of modulating much faster, it is limited by its polarization maintaining design and low power threshold. In the method of pump modulation, no intra-cavity modulator is necessary. Cavity gain is modulated by directly modulating the pump power, instead of modulating cavity loss, as shown Figure 4.2. Therefore this method provides a low-loss and simple design for active mode locked fiber laser.

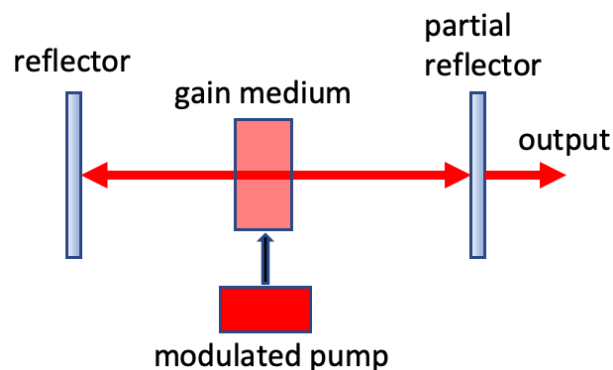


Figure 4.1: Schematic of active mode locking by pump modulation

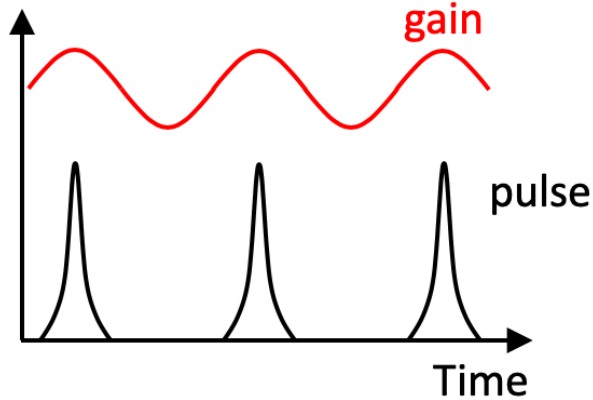


Figure 4.2: Active mode locking by pump modulation in time domain

4.2 Previous Work on Active Mode Locking via Pump Modulation

This thesis mainly focuses on Yb-doped mode locked fiber laser via pump modulation. The method of pump modulation has been realized previously in Tm-doped fiber laser and Er-doped fiber laser. In this section, we introduce the previous work on AMPM.

4.2.1 Thulium-doped Mode Locked Fiber Laser via Pump Modulation

The method of AMPM was firstly realized in Tm-doped fiber laser [16]. Experimental setup is shown in Figure 4.3. The seed pump laser was firstly modulated with sinusoidal waveform, and then amplified by an EDFA. Tm-doped fiber used was 4 m (TmDF200, from OFS). Total cavity length was estimated to be 16 m, corresponding to a repetition rate of 12.9 MHz.

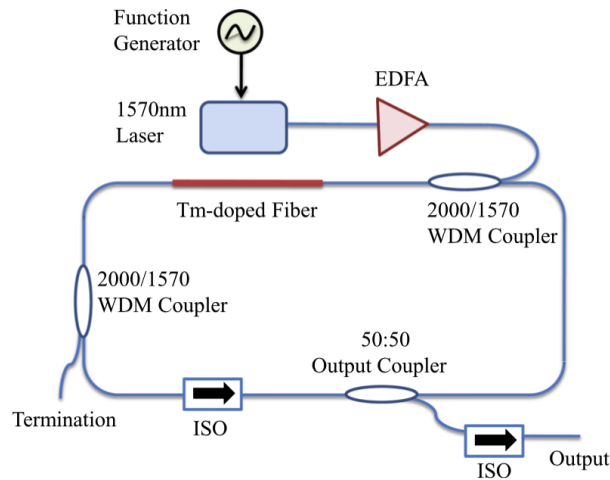


Figure 4.3: Active mode locking via pump modulation in Tm-doped fiber laser [16]

CW mode locking could be achieved by setting the modulation index to be 30% and

modulation frequency at 12.8728 MHz. Signal modulation index was estimated to be 0.01%. Results were shown in Figure 4.4. Spectral bandwidth was measured to be 0.9 nm with resolution of 0.5 nm, as shown in Figure 4.4 (a). Pulse width was measured to be 4.4 ps assuming a hyperbolic-secant pulse shape, as shown in Figure 4.4 (b). Time-bandwidth product was calculated to be 0.31, close to the transform limit of soliton pulse (0.315). Signal to noise ratio (SNR) was 63 dB with a resolution bandwidth of 300 Hz. Pump power threshold for mode locking was around 100 mW, and output was 20 mW when pump power was set to 400 mW.

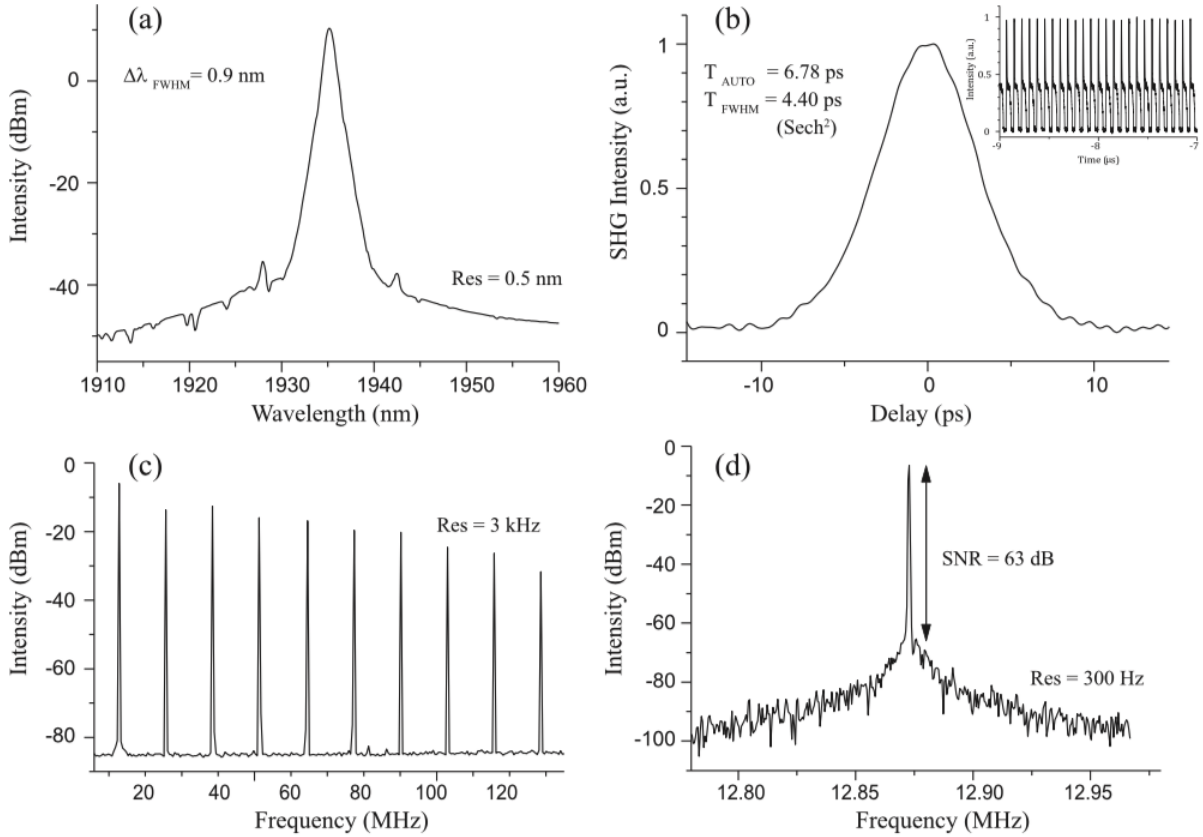


Figure 4.4: Experiment results. (a) Output spectrum; (b) autocorrelation trace (inset: oscilloscope waveform); (c) and (d) RF spectrum. [16]

Second-harmonic mode locking is also achieved by doubling the modulation frequency to 25.7560 MHz, as shown in Figure 4.5. Spectral width and pulse width were 0.83 nm and 4.7 ps respectively as shown in Figure 4.5 (a) and (b), giving a time-bandwidth product of 0.37. SNR was measured to be 55 dB at mode locking frequency (Figure 4.5 (d)) and weak signal at fundamental frequency was also observed (Figure 4.5 (c)).

4.2.2 Erbium-doped Mode Locked Fiber Laser via Pump Modulation

AMPM was also used to mode lock an Er-doped fiber laser [17]. Experimental setup is shown in Figure 4.6. 980 nm pump laser was directly modulated by a laser driver with

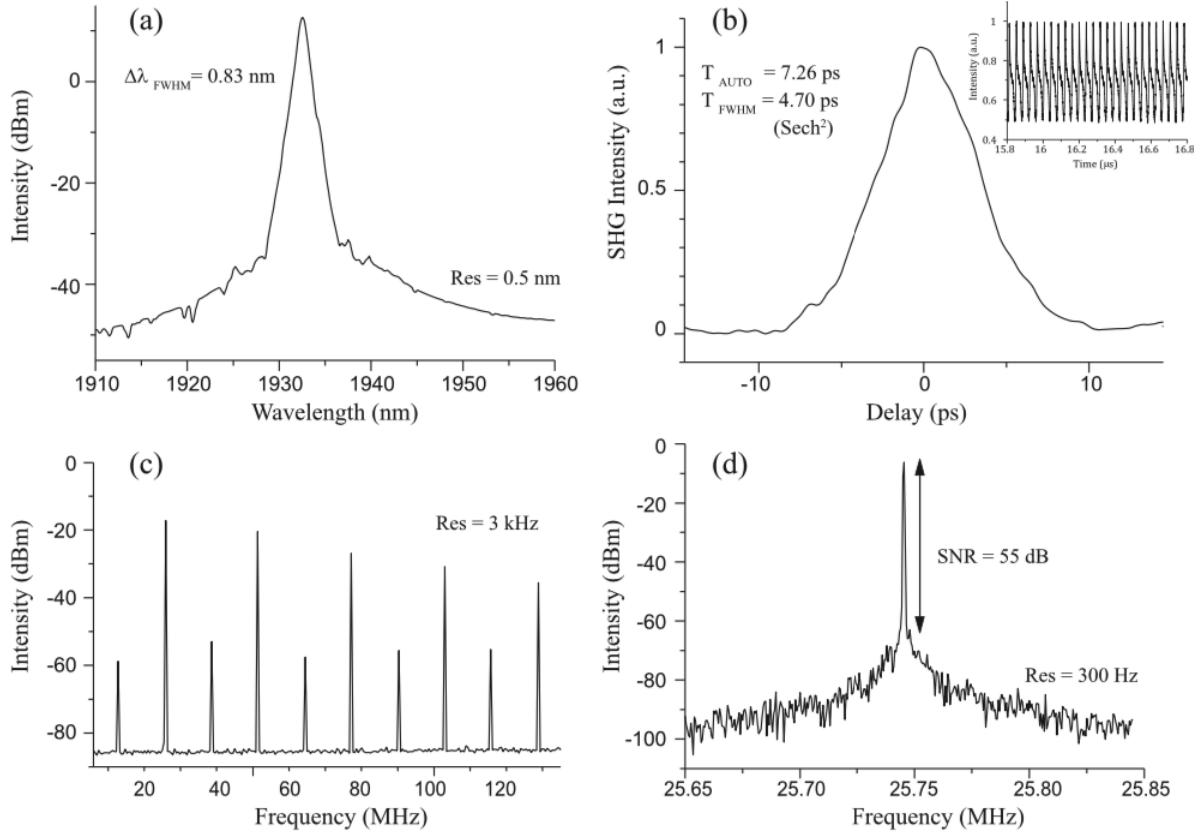


Figure 4.5: Second-harmonic mode locking experiment results. (a) Output spectrum; (b) autocorrelation trace (inset: oscilloscope waveform); (c) and (d) RF spectrum. [16]

sinusoidal waveform. Length of Er-doped fiber is 0.4 m. 2 km dispersion shift fiber (DSF) was used to elongate the cavity length without changing total cavity dispersion. Cavity length other than DSF was around 16 m. Total cavity dispersion was estimated to be -0.31 ps^2 .

CW mode locking was achieved by setting the modulation frequency at 99.021 kHz and modulation index at 91%. Results are shown in Figure 4.7. Figure 4.7 (a) shows the optical spectrum with bandwidth of 2.26 nm. Figure 4.7 (b) shows the RF spectrum of the pulse train. SNR was measured to be 53 dB with resolution bandwidth of 100 Hz. Figure 4.7 (c) shows the pulse autocorrelation trace with a pulse width of 1.18 ps assuming hyperbolic-secant pulse shape, giving a time-bandwidth product of 0.387. Output power was 10 mW when pump power was set at 548 mW.

By using only 1 km DSF, mode locking could also be achieved, with spectral bandwidth of 2.27 nm, repetition rate of 197.000 kHz and pulse width of 1.12 ps.

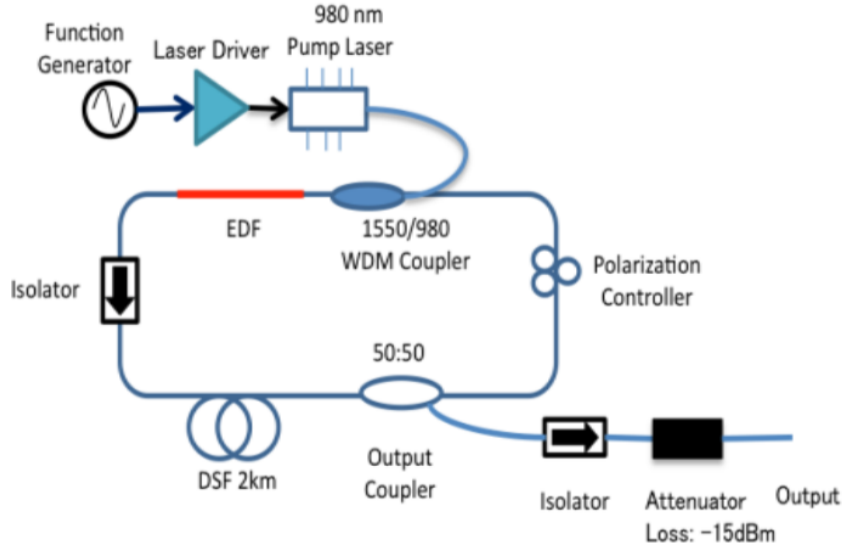


Figure 4.6: Active mode locking via pump modulation in Tm-doped fiber laser [17]

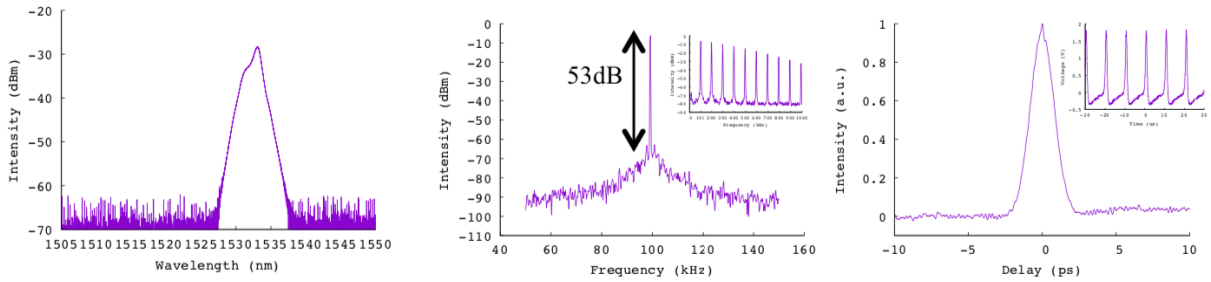


Figure 4.7: Experiment results. (a) Output spectrum; (b) PF spectrum; (c) autocorrelation trace. [17]

4.3 Ytterbium Doped Mode Locked Fiber Laser via Pump Modulation

In this section, our experiments on Yb-doped mode locked fiber laser via pump modulation will be presented. Firstly, we explored the feasibility of pump modulation method at all normal dispersion configuration. Results showed its infeasibility due to weak modulation index. To increase modulation index, we inserted 1 *km*-long passive fiber into the cavity to lower down the cavity repetition rate. Pulsing was observed in this experiment while results and analysis indicated a noise-like pulse rather than a mode locked pulse. Finally, we attempted to introduce dispersion compensation in the cavity. When cavity net dispersion was compensated to small and normal, extremely unstable pulse train could be observed. Stable pulse train could not be produced.

4.3.1 All Normal Dispersion Configuration

Experiments and results

Different from Tm-doped fiber and Er-doped fiber, fiber exhibits normal dispersion at lasing wavelength of Yb-doped fiber. As has been introduced in Chapter 2, section 2.4, to mode lock an all normal dispersion fiber laser, strong modulation index is necessary. In this attempt, we try to modulate the laser without any dispersion compensation.

The experimental setup for all normal dispersion configuration is shown in Figure 4.8. 980 nm pump laser was modulated by a laser driver. Yb-doped fiber (SM-YSF-HI, from Nufern) was around 1.5 m. Terminator connected to a WDM was used to block the residual pump. A polarization-independent isolator (PI-ISO) ensured the unidirectional operation of the laser. Output coupler coupled 10% cavity light out of the cavity as laser output.

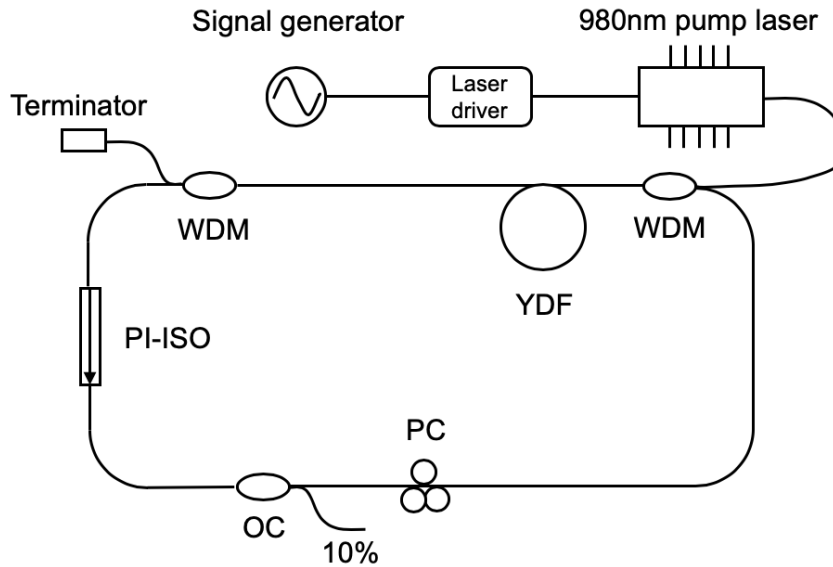


Figure 4.8: Experimental setup for all normal dispersion configuration

By tuning the modulation frequency to cavity repetition rate, CW output was observed instead of mode locking, which was anticipated since gain modulation transfer was extremely low (around 0.01%) at modulation frequency of around 10 MHz (refer to measurement results in Chapter 3, Section 3.2).

Spectral filtering can also lead to amplitude modulation to help shaping the pulse [25]. In our experiment, we also tried to insert bandpass filter with 2 nm and 8 nm bandwidth in the cavity, but mode locking was still not achieved.

Next, we conduct numerical simulation to verify that modulation index is determinant to pulse shaping at all normal dispersion.

Numerical simulation

Numerical simulation was conducted following the method in Chapter 2, section 2.5. Two points should be addressed in the simulation below. Firstly, as Equation 2.5 shows, gain g and loss α have the same position in the equation. Therefore we make the assumption that loss α is modulated rather than gain g , for the sake of simplicity. Secondly, loss modulation

4.3. YTTERBIUM DOPED MODE LOCKED FIBER LASER VIA PUMP MODULATION

is assumed to be instantaneously (length of the loss modulator can be neglected). Loss modulation function is given by:

$$T = 1 - m + m \cos 2\pi\omega_f t \quad (4.1)$$

where T is the transmission, m is the modulation depth and ω_f is the modulation frequency. By taking its Taylor series at $t = 0$, and only considering the first two orders, we have:

$$T \approx 1 - 2\pi^2 m \omega_f^2 t^2 \quad (4.2)$$

Flow diagram of the simulation is shown in Figure 4.9. Simulation starts from noise. Light passes through single mode fiber (SMF), Yb-doped fiber (YDF), amplitude modulation and optical coupler (OC) as one single loop. 50,000 iterations were executed in each simulation. Simulation parameters are given in Table 4.1. We investigated pulse shaping as modulation index m varies ($m = 1/2^i$, $i = 0, 1, 2, \dots, 14$).

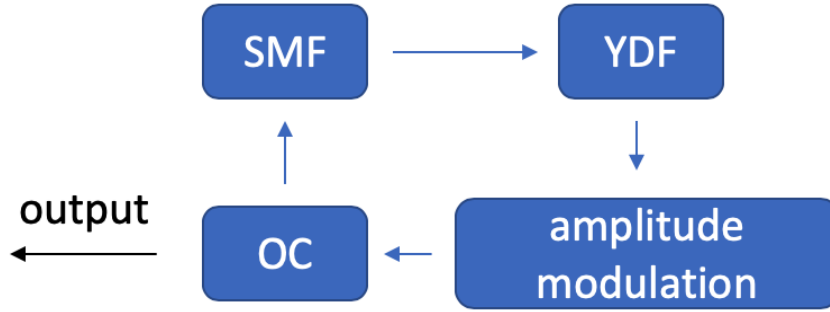


Figure 4.9: Flow diagram of the simulation

Table 4.1: Parameters in simulation

Parameter	Value
l_{smf}	12 m
β_{2_smf}	0.017 ps ² /m
γ_{smf}	0.00544 /W/m
l_{ydf}	4 m
β_{2_ydf}	0.025 ps ² /m
γ_{ydf}	0.0058 /W/m
g_s	30 dB
E_s	0.5 pJ
gain bandwidth	80 nm
m	$1/2^i$, ($i = 0, 1, 2, \dots, 14$).
coupling ratio	50%

Simulation results show that stable pulse can be formed when modulation index take these value: $m = 1/2^i$, $i = 0, 1, 2, \dots, 6$. Noise-like pulse is observed when $m = 1/2^i$, $i = 7, 8, 9, 10$. Pulse can not be formed when $m = 1/2^i$, $i = 11, 12, 13, 14$.

Figure 4.10 and 4.11 show the simulation results of stable mode locking when modulation index $m = 1/2^i$, $i = 0, 1, 2, \dots, 6$. As modulation index decreases, pulse peak power decreases and pulse width increases significantly, suggesting that modulation index has great importance on pulse shaping at normal dispersion. Higher modulation index is capable of shaping the pulse more effectively, leading to a narrower output pulse. Besides, spectral bandwidth decreases as modulation index decreases.

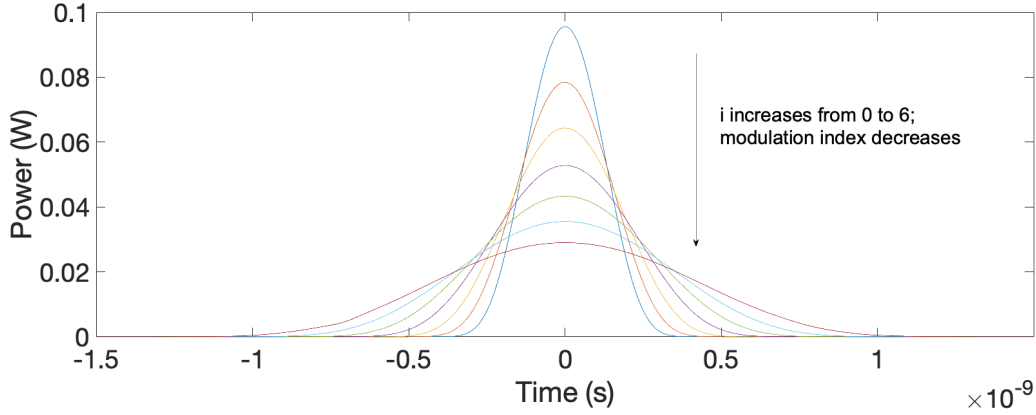


Figure 4.10: Simulation result: pulse shape when modulation index $m = 1/2^i$, $i = 0, 1, 2, \dots, 6$

Figure 4.12 and 4.13 show the simulation results of noise-like pulse when modulation index $m = 1/2^i$, $i = 7, 8, 9, 10$. As modulation index decreases, pulse becomes more noisy, and spectral bandwidth becomes narrower. It indicates that when modulation index is too weak, pulse is can not be stabled.

Figure 4.14 and 4.15 show the simulation results of noise when modulation index $m = 1/2^i$, $i = 11, 12, 13, 14$. In this case, modulation index is so low that pulse can not be formed.

In summary, we show that modulation index is determinant to pulse forming and shaping at all normal dispersion configuration. Strong modulation index can help to form the pulse effectively. The stronger the modulation is, the narrower the pulse will be. At weak modulation index, pulse can not be stabilized, or can not be formed.

Conclusion

Based on the experiment results and simulations above, it can be concluded that Yb-doped mode locked fiber laser is not feasible at 10 MHz repetition rate or higher. Infeasibility can be attributed to weak modulation index.

4.3. YTTERBIUM DOPED MODE LOCKED FIBER LASER VIA PUMP MODULATION

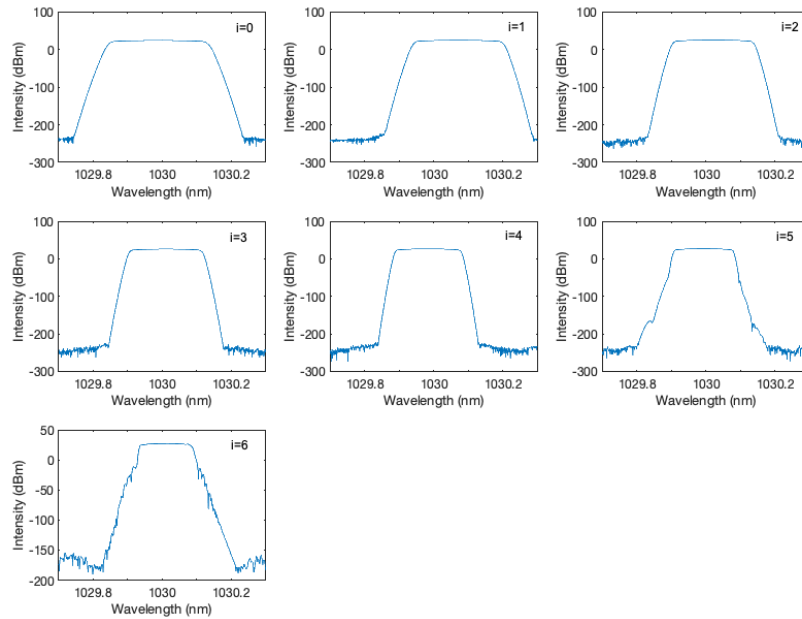


Figure 4.11: Simulation result: spectrum when modulation index $m = 1/2^i$, $i = 0, 1, 2, \dots, 6$

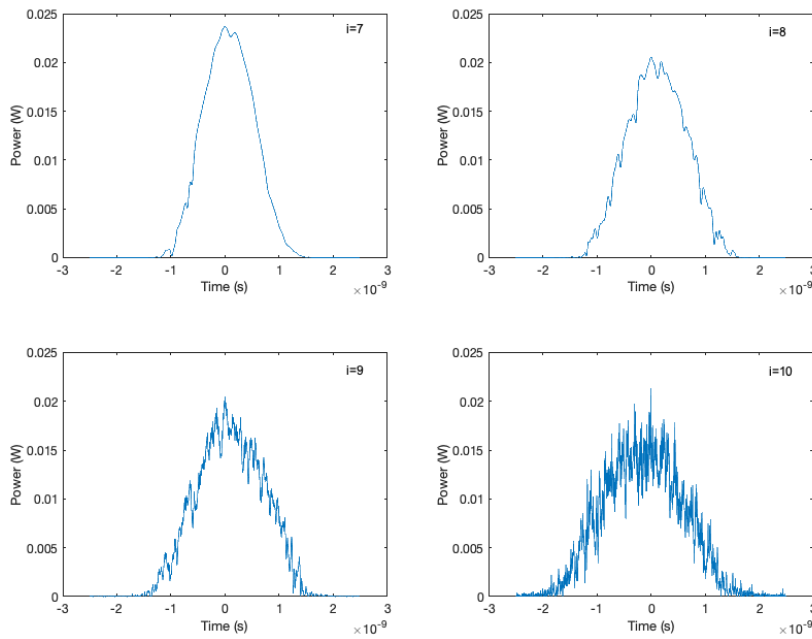


Figure 4.12: Simulation result: pulse shape when modulation index $m = 1/2^i$, $i = 7, 8, 9, 10$

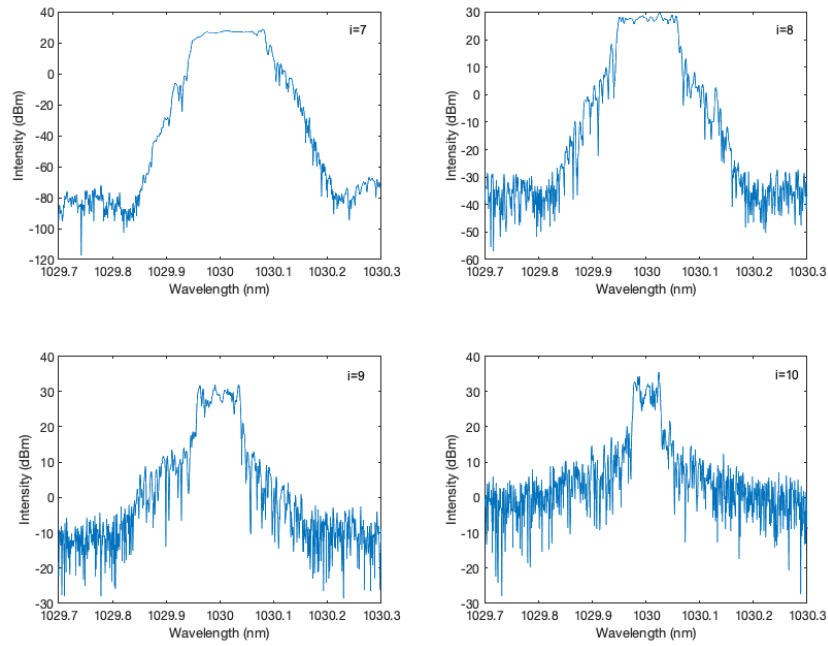


Figure 4.13: Simulation result: spectrum when modulation index $m = 1/2^i$, $i = 7, 8, 9, 10$

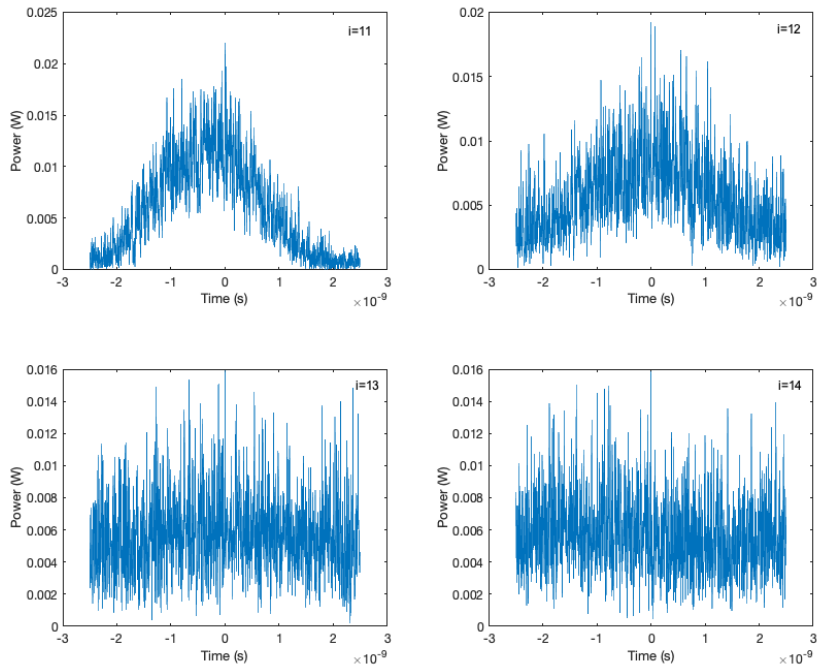


Figure 4.14: Simulation result: temporal output when modulation index $m = 1/2^i$, $i = 11, 12, 13, 14$

4.3. YTTERBIUM DOPED MODE LOCKED FIBER LASER VIA PUMP MODULATION

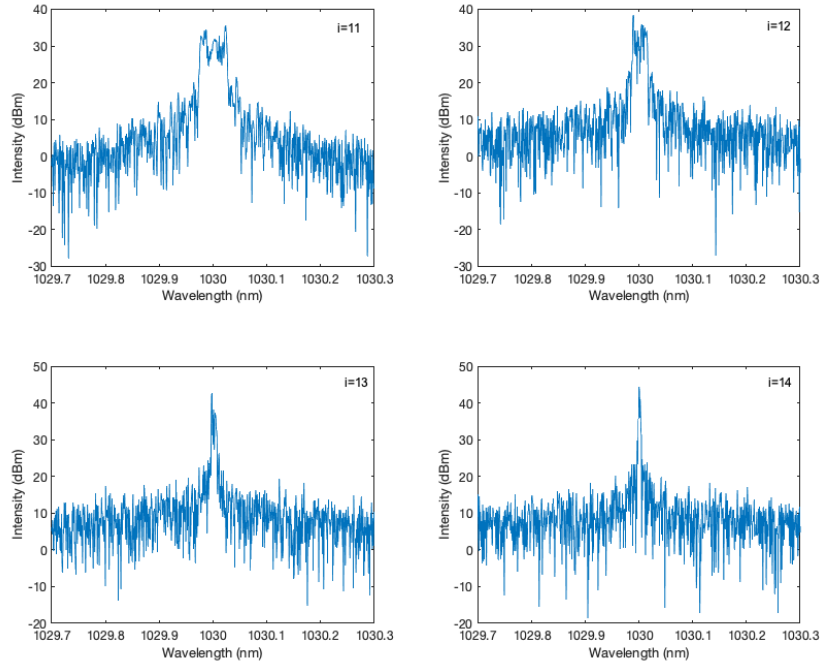


Figure 4.15: Simulation result: spectrum when modulation index $m = 1/2^i$, $i = 11, 12, 13, 14$

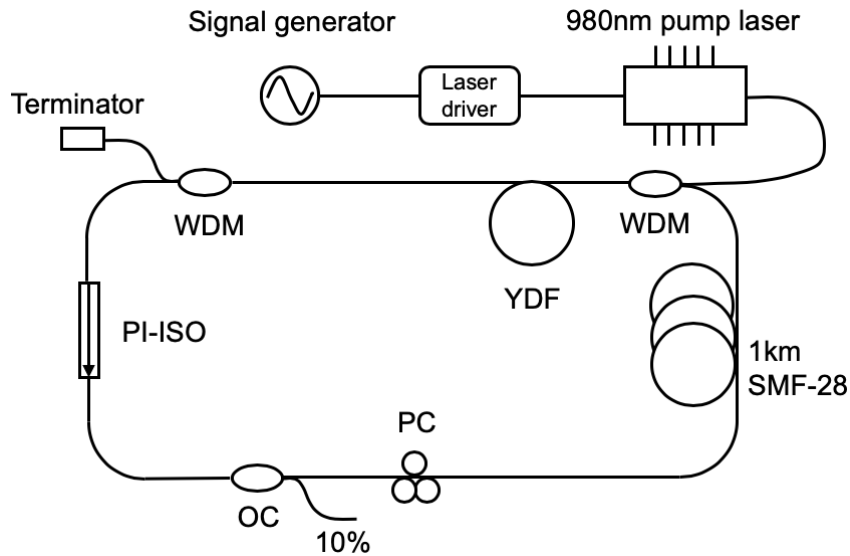


Figure 4.16: Experimental setup for all normal dispersion configuration with kilometer-long cavity

4.3.2 All Normal Dispersion Configuration with Kilometer-long Cavity

Experiment and result

In order to increase the modulation index, we increased the length of laser cavity by inserting 1 *km* standard single mode fiber (SMF28), lowering the modulation frequency down to around 200 kHz. Experimental setup is shown in Figure 4.16. Except 1 *km* SMF-28, rest of the cavity is the same as Figure 4.8. Modulation index transfer was estimated to be 0.5% according to the measurements in Chapter 3, Section 3.2.

Pulsing was observed when modulation frequency was tuned from 199.022 kHz to 199.284 kHz. Pulse was measured with a PD (Model: DET08CFC/M, 5 GHz, from THORLABS), and a 200 MHz oscilloscope, as shown in Figure 4.17. Pulse width was measured to be around 500 *ns*. Spectrum was shown in Figure 4.18, with 3 dB bandwidth of 2.5 *nm*.

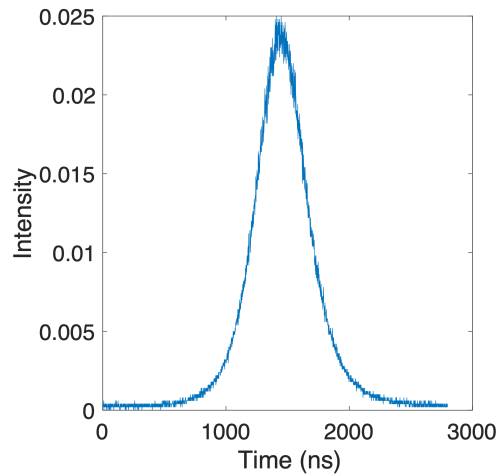


Figure 4.17: Output pulse measured by PD and oscilloscope. Pulse width: 500 *ns*

Pulse characterization

The pulse width was so large that it could not be characterized by autocorrelator. Whether the pulse was mode locked should be verified by other means. Assuming that the pulse was mode locked, the pulse should be highly chirped at this kilometer-long all normal dispersion configuration. Therefore the pulse should be broadened or compressed after passing through dispersive fiber. Here, we launched the pulse into a segment of 500 *m* SMF-28, and checked whether the pulse width changed. Results are shown in Figure 4.19. Left side of the figure shows the optical spectrum before and after dispersive fiber. Spectrum did not change significantly, meaning that nonlinearity effect could be neglected and only dispersion was responsible for any possible pulse shape change. However, as right side of the figure shows, normalized pulse shape and pulse width were not changed significantly, indicating that the pulse was not chirped as expected.

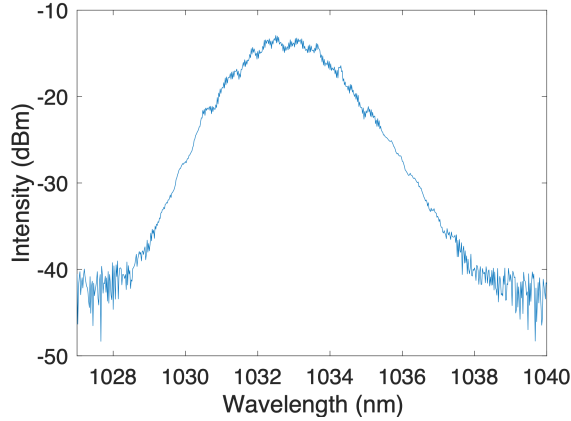


Figure 4.18: Output spectrum. 3 dB bandwidth: 2.5 nm

Degree of polarization (DOP) of the output was also measured with a polarimeter (PAX1000IR2/M, from THORLABS). When modulation frequency was tuned to cavity repetition rate, output was pulsing and DOP was only around 18%. However when it was detuned, output become CW and DOP become significantly higher, up to 65%. Physical mechanism of this observation is unclear yet.

Conclusion

Based on the analysis above, it can be concluded that the produced pulse was not mode locked pulse. One possible explanation is that the output pulse may be the pulsing of amplified spontaneous emission (ASE). If this is the case, however, the reason for why ASE rather than lasing was produced in a closed ring cavity is unclear.

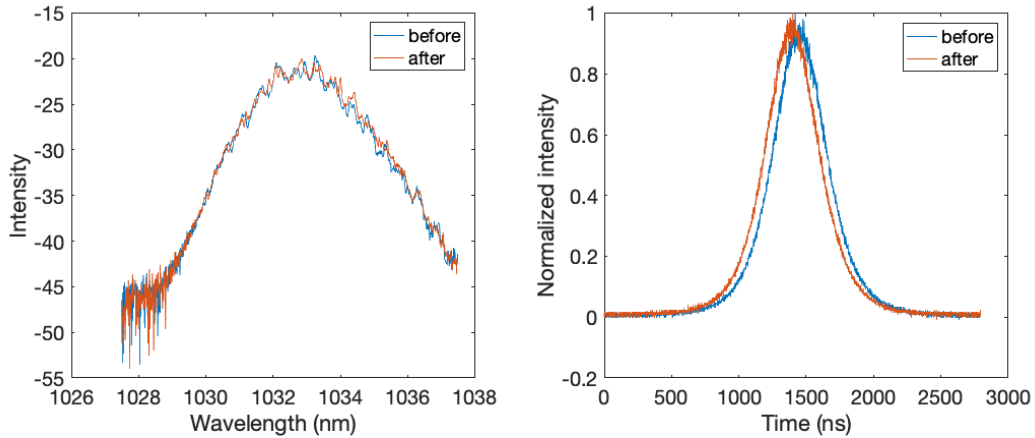


Figure 4.19: Spectrum (left) and normalized temporal shape (right) before (blue) and after (red) passing through 500 m SMF-28

4.3.3 Dispersion Compensated Configuration

It is usually difficult to mode lock a fiber laser at all normal dispersion. Compensating certain amount of anomalous dispersion can help to form the pulse [24]. Stretched pulse (also known as dispersion managed soliton) is formed when net dispersion is small and normal, or small and anomalous. As we failed to mode lock the laser at all normal dispersion, we investigated the feasibility of dispersion compensated configuration. Experimental setup is shown in Figure 4.20. Total cavity length was around 19 m. Yb-doped fiber (SM-YSF-HI, from Nufern) was around 1.5 m. Dispersion compensation was provided by grating pair (refer to Appendix for dispersion compensation with grating pair). Grating used in the experiment was transmission type, with line density of 1000 lines/mm and incident angle of $31.3 \pm 1^\circ$ (T-1000-1040, from LightSmyth). Light was coupled out of fiber and into fiber by two fiber pigtail collimators. After light is dispersed, it gets reflected by a total reflection mirror M2. Then, light passes through grating pair again and gets dispersed again. Finally, light is reflected by a total reflection mirror M1 and coupled back into fiber.

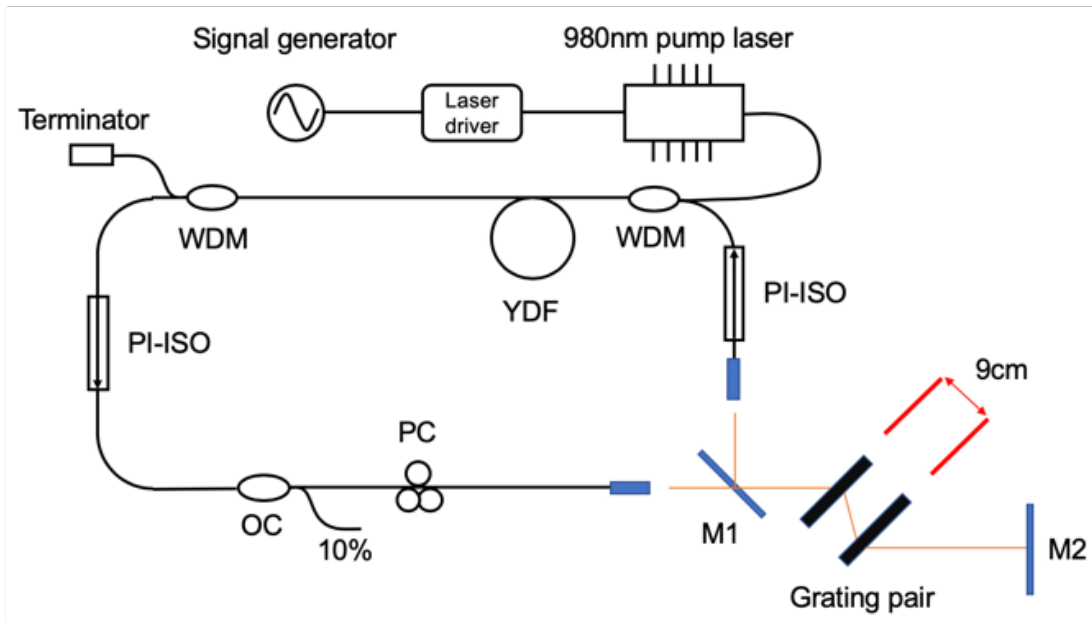


Figure 4.20: Experimental setup for dispersion compensated configuration

When grating spacing was around 9 cm, cavity net dispersion was calculated to be around 0.0615 ps^2 . Extremely unstable pulse train could be observed when modulation frequency was tuned to cavity repetition rate, as shown in Figure 4.21. The pulse was so unstable that it could not be characterized by autocorrelator. Stable pulsing was not achieved.

In gain modulation, there is modulation index fluctuation and high-order modulation fluctuation due to noise from the modulated pumping. Unlike soliton pulse where pulse shaping was achieved by only nonlinearity and anomalous dispersion, modulation index is determinant for pulse shaping in this experiment. Therefore, any possible fluctuation of modulation index and high-order modulation fluctuation would lead to unstableness. In

4.3. YTTERBIUM DOPED MODE LOCKED FIBER LASER VIA PUMP MODULATION

our experiment, the amount of modulation index was still not strong enough to counter against the noise. Besides, the unstableness might also be attributed to modulation frequency detuning since cavity length was environmental sensitive.



Figure 4.21: One frame of unstable pulse train footage

4.3.4 Conclusion

Results show the infeasibility of Yb-doped mode locked fiber laser via pump modulation. Mode locking was not produced. At normal dispersion, modulation index is determinant for pulse forming. However at around 10 MHz modulation frequency (20 m-long cavity), modulation index transfer is only around 0.01% according to the measurements in Chapter 3, Section 3.2. Such low modulation index is not capable of forming the pulse effectively shown by simulation. Besides, stable mode locking can not be produced by compensating cavity dispersion.

Chapter 5

Conclusion and Future Work

5.1 Conclusion

In this thesis, we investigated Yb-doped mode locked fiber laser by the method of modulating pump. As the fundamentals of pump modulation method, we characterized the pump to signal transfer of modulation index in gain fiber. Experimental results indicated that the transfer of modulation index exhibited low-pass filter characteristics, which matched well with theoretical model.

Three configurations were tried to mode lock the Yb-doped fiber laser. With all normal dispersion configuration, only CW output could be produced. Simulation was conducted with varying modulation index. It showed that modulation index was determinant for pulse forming at normal dispersion. In the experiment, reason for not pulsing could be attributed to weak modulation index at high modulation frequency.

To increase modulation index, cavity repetition rate was lowered down to around 200 kHz by inserting 1 *km*-long fiber into the cavity. Pulse was produced with this configuration. However, analysis showed that it was not mode locked pulse. Physical mechanism of this observation still remains to be explored.

Efforts were also made to mode lock the laser with dispersion compensation. Extremely unstable pulse train was produced when cavity net dispersion was compensated to small and normal. However stable pulse train could not produced. The unstableness was attributed to modulation index fluctuation and high-order modulation fluctuation due to noise from the modulated pumping. Besides, unstableness might also be because of frequency detuning caused by environmental sensitive cavity length change.

In summary, although the method of AMPM showed its feasibility and advantage in Tm and Er-doped mode locked fiber laser, it can be concluded that this method does not apply well to Yb-doped mode locked fiber laser due to low modulation index transfer and normal dispersion.

5.2 Future Work

Results showed that pump modulation might not be an effective pulse shaper for Yb-doped fiber laser. However, it may be helpful to start a mode locked laser. For some passive mode locked fiber lasers, self-starting is a critical issue. One way to start the

pulsing is to increase the pump power. But the pulse produced may suffer from pulse breaking and multiple pulse because the pump power is high. It is also possible to start pulsing by mechanically vibrating the fiber cavity to introduce perturbation. Considering that pump modulation is a reliable way of introducing perturbation, there is a great potential that this method is promising for starting a passive mode locked fiber laser or lowering down the mode locking threshold. As for our future work, we will try to apply pump modulation to a figure-8 Yb-doped mode locked fiber laser with high mode locking threshold, and study the effect of pump modulation on mode locking threshold and pulse starting.

Appendix

Pulse Propagation Equation

Optical fields in optical fibers follow the rule of Maxwell's equations as follows:

$$\nabla \times \mathbf{E} = -\frac{\partial \mathbf{B}}{\partial t} \quad (5.1)$$

$$\nabla \times \mathbf{H} = \mathbf{J} + \frac{\partial \mathbf{D}}{\partial t} \quad (5.2)$$

$$\nabla \cdot \mathbf{D} = \rho_f \quad (5.3)$$

$$\nabla \cdot \mathbf{B} = 0 \quad (5.4)$$

where \mathbf{E} and \mathbf{H} are electric and magnetic fields respectively, and \mathbf{D} and \mathbf{B} are electric and magnetic flux densities. \mathbf{J} is the current density vector and ρ_f is charge density. In optical fibers, $\mathbf{J} = 0$ and $\rho_f = 0$. \mathbf{D} and \mathbf{B} are related with to \mathbf{E} and \mathbf{H} in the following equations:

$$\mathbf{D} = \epsilon_0 \mathbf{E} + \mathbf{P} \quad (5.5)$$

$$\mathbf{B} = \mu_0 \mathbf{H} + \mathbf{M} \quad (5.6)$$

where ϵ_0 is the vacuum permittivity and μ_0 is the vacuum permeability. \mathbf{P} and \mathbf{M} are induced electric and magnetic polarization. In optical fiber, \mathbf{M} can be neglected.

By Eqs (5.1), (5.2), (5.3), (5.5) and (5.6), we can derive the following equation:

$$\nabla^2 \mathbf{E} = \frac{1}{c^2} \frac{\partial^2 \mathbf{E}}{\partial t^2} + \mu_0 \frac{\partial^2 \mathbf{P}}{\partial t^2} \quad (5.7)$$

If we write \mathbf{P} as the sum of its linear part \mathbf{P}_L and nonlinear part \mathbf{P}_{NL} , we have:

$$\mathbf{P} = \mathbf{P}_L + \mathbf{P}_{NL} \quad (5.8)$$

By using Eqs (5.7) and (5.8), we have:

$$\nabla^2 \mathbf{E} - \frac{1}{c^2} \frac{\partial^2 \mathbf{E}}{\partial t^2} = \mu_0 \frac{\partial^2 \mathbf{P}_L}{\partial t^2} + \mu_0 \frac{\partial^2 \mathbf{P}_{NL}}{\partial t^2} \quad (5.9)$$

Here, we separate the slowly varying envelop and rapidly varying part of the electric field and its polarization components, as follows:

$$\mathbf{E}(\mathbf{r}, t) = \frac{1}{2} \vec{x} [E(\mathbf{r}, t) \exp(-i\omega_0 t) + c.c.] \quad (5.10)$$

$$\mathbf{P}_L(\mathbf{r}, t) = \frac{1}{2}\vec{x}[P_L(\mathbf{r}, t) \exp(-i\omega_0 t) + c.c.] \quad (5.11)$$

$$\mathbf{P}_{NL}(\mathbf{r}, t) = \frac{1}{2}\vec{x}[P_{NL}(\mathbf{r}, t) \exp(-i\omega_0 t) + c.c.] \quad (5.12)$$

P_L and P_{NL} can be expressed as:

$$P_L(\mathbf{r}, t) = \frac{\epsilon_0}{2\pi} \int_{-\infty}^{\infty} \tilde{\chi}_{xx}^{(1)}(\omega) \tilde{E}(\mathbf{r}, \omega - \omega_0) \exp[-i(\omega - \omega_0)t] d\omega \quad (5.13)$$

$$P_{NL}(\mathbf{r}, t) \approx \epsilon_0 \epsilon_{NL} E(\mathbf{r}, t) \quad (5.14)$$

Here, $\tilde{E}(\mathbf{r}, \omega - \omega_0) = \int_{-\infty}^{\infty} E(\mathbf{r}, t) \exp[i(\omega - \omega_0)t] dt$ is the Fourier transform of $E(\mathbf{r}, t)$, $\epsilon_{NL}(\mathbf{r}, t) = \frac{3}{4}\chi_{xxxx}^{(3)}|E(\mathbf{r}, t)|^2$.

By Eqs (5.9)-(5.14), we have \tilde{E} satisfying the Helmholtz equation:

$$\nabla^2 \tilde{E} + \epsilon(\omega) k_0^2 \tilde{E} = 0 \quad (5.15)$$

Eq (5.15) can be solved by the method of separation of variables. We write \tilde{E} in the following form:

$$\tilde{E}(\mathbf{r}, \omega - \omega_0) = F(x, y) \tilde{A}(z, \omega - \omega_0) \exp(i\beta_0 z) \quad (5.16)$$

where \tilde{A} is the slowly varying electric field envelop as a function of z . $F(x, y)$ is the transverse mode distribution in optical fiber. By substituting Eq (5.16) into Eq (5.15) and ignoring cubic and higher-order terms of $\beta(\omega)$, we can solve for A , described by the following equation:

$$\frac{\partial A}{\partial z} + \beta_1 \frac{\partial A}{\partial t} + \frac{i\beta_2}{2} \frac{\partial^2 A}{\partial t^2} + \frac{\alpha}{2} A = i\gamma |A|^2 A \quad (5.17)$$

Here, β_1 and β_2 are the first order and second order chromatic dispersion. α is fiber loss and γ is fiber nonlinearity. By defining $T = t - \beta_1 z$ and substituting it into Eq (5.17), we can eliminate β_1 , and get pulse propagation equation with T as a moving frame at the pulse propagation speed $1/\beta_1$:

$$\frac{\partial A}{\partial z} + \frac{i\beta_2}{2} \frac{\partial^2 A}{\partial T^2} + \frac{\alpha}{2} A = i\gamma |A|^2 A \quad (5.18)$$

MATLAB code for simulating pulse propagation in gain fiber

Here we present the MATLAB simulation code for pulse propagation in gain fiber described by Eq. (2.5).

```

1 clear;
2 clc;
3 l = 0; % fiber loss
4 gs = 30; % small signal gain, dB/m
5 gs = gs/10*log(10);
6 l_gf = 4; % gain fiber length, m
7 seg_gf = 100; % segments of gain fiber
8 b2_gf = -0.02e-24; % GVD of gain fiber, S^2/s
9 gamma_ydf = 5.3e-3; % SPM of gain fiber, /W/m
10 E_sat = 0.5e-12; % gain fiber saturation energy, J
11
12 lambda0 = 1530e-9; % central wavelength, m
13 span = 100e-12; % simulation window, s
14 n = 2^12; % sampling points in simulation window
15 dt = span/n;
16 t = linspace(-n/2, n/2-1, n)*dt;
17 A = 10^-9*gaussmf(t, [100*dt, 0]); % input pulse in Gaussian shape
18 dw = 2*pi/span;
19 w = linspace(-n/2, n/2-1, n)*dw;
20 lambda = 2*pi*3e8./(2*pi*3e8/lambda0+w);
21 lambda = lambda(end:-1:1);
22
23 bw_gain = 45e-9; % gain bandwidth, m
24 a = 0.5/(bw_gain/2)^2;
25 g_w = -1*a*(lambda-lambda0).^2+1; % wavelength dependency of gain, in ...
    parabolic shape
26 g_w(g_w<0) = 0;
27
28 %%Pulse propagation, by split-step Fourier method%%
29 for i=1:seg_gf
30     W = sum(abs(A).^2)*dt; % pulse energy
31     g = gs./(1+W/E_sat); % saturated gain
32     D = -1j/2*b2_gf*(-1j*w).^2+g*g_w; % dispersion operator in ...
    split-step Fourier method
33     B = fftshift(fft(ifftshift(A))); % Fourier transform of A
34     B = B.*exp(D*l_gf/seg_gf);
35     A = fftshift(ifft(ifftshift(B))); % inverse Fourier transform of B
36     N = 1j*gamma_gf*abs(A).^2; % nonlinear operator in split-step ...
    Fourier method
37     A = A.*exp(N*l_gf/seg_gf);
38 end

```

Dispersion Compensation with Grating Pair

Grating pair can provide anomalous dispersion, by creating path difference among different frequencies, as shown in Figure 5.1. When light is incident on the grating at incident angle θ_i , light will be dispersed to different angles by its frequency:

$$\sin \theta_m = m \frac{\lambda}{\Lambda} + \sin \theta_i \quad (5.19)$$

where m is diffraction order, λ is wavelength of light, Λ is line spacing and θ_m is m -th order diffraction angle. First order diffraction is usually adopted because it has the highest diffraction efficiency.

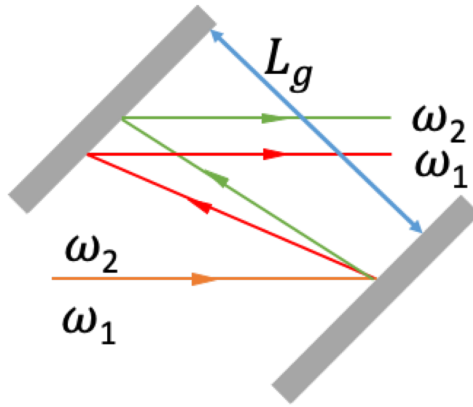


Figure 5.1: Grating pair for dispersion compensation

By placing two gratings in parallel, angular dispersion can be transformed into path difference. Assuming the spacing of the grating pair is L_g , dispersion β_2 provided by the grating pair is given by:

$$\beta_2 = -\frac{m^2 \lambda^3 L_g}{4\pi c^2 \Lambda^2} \left[1 - \left(-m \frac{\lambda}{\Lambda} - \sin \theta_i \right)^2 \right]^{-3/2} \propto L_g \quad (5.20)$$

where c is the speed of light. It shows that dispersion provided by grating pair is proportional to grating spacing.

Acknowledgments

First of all, I would like to thank my supervisor, professor Shinji Yamashita for consistent support in my research. His helpful advice and insightful opinions always inspire me during my study. Moreover, he is an admirable person of integrity. His attitude towards research and people keeps guiding me to become a better person.

I would also like to thank professor Sze Yun Set, who is always encouraging me and provides lots of help on my experiments. He is humorous, easy-going and talented. His scientific spirit greatly helps me to shape my way of thinking towards problems.

Besides, I would also like to appreciate Dr. Lei Jin, Dr. Yohei Sugiura, Takuma Shirahata, Hongbo Jiang, Zheyuan Zhang, Shoko Yokokawa, Pengtao Yuan and Sifan Liu. They helped me a lot on my daily life and study.

Specially, I would like to express my sincere gratitude to MERIT-WINGS program of the University of Tokyo and my sub-supervisor for the program, professor Takashi Kondo for not only financial support, but also offering me an interdisciplinary training.

Finally, I would like to thank my family for their generous dedication and support for everything.

Bibliography

- [1] F. J. McClung and R. W. Hellwarth. Giant optical pulsations from ruby. *Journal of Applied Physics*, 33(3):828–829, 1962.
- [2] L. E. Hargrove, R. L. Fork, and M. A. Pollack. Locking of he–ne laser modes induced by synchronous intracavity modulation. *Applied Physics Letters*, 5(1):4–5, 1964.
- [3] Y. Jeong, J. K. Sahu, D. N. Payne, and J. Nilsson. Ytterbium-doped large-core fiber laser with 1 kw continuous-wave output power. In *Advanced Solid-State Photonics*, page PDP13. Optical Society of America, 2004.
- [4] Russell L. McCally, C. Brent Barger, Jennifer A. Bonney-Ray, and W. Richard Green. Laser eye safety research at apl. *Johns Hopkins APL Technical Digest (Applied Physics Laboratory)*, 26(1):46–54, 1 2005.
- [5] Peifang Tian, Dorine Keusters, Yoshifumi Suzaki, and Warren S. Warren. Femtosecond phase-coherent two-dimensional spectroscopy. *Science*, 300(5625):1553–1555, 2003.
- [6] Ajay Nahata, Aniruddha S. Weling, and Tony F. Heinz. A wideband coherent terahertz spectroscopy system using optical rectification and electro-optic sampling. *Applied Physics Letters*, 69(16):2321–2323, 1996.
- [7] Yasuyuki Ozeki, Wataru Umemura, Yoichi Otsuka, Shuya Satoh, Hiroyuki Hashimoto, Kazuhiko Sumimura, Norihiko Nishizawa, Kiichi Fukui, and Kazuyoshi Itoh. High-speed molecular spectral imaging of tissue with stimulated raman scattering. *Nature Photonics*, 6:845 EP –, Nov 2012. Article.
- [8] Warren R. Zipfel, Rebecca M. Williams, and Watt W. Webb. Nonlinear magic: multi-photon microscopy in the biosciences. *Nature Biotechnology*, 21(11):1369–1377, 2003.
- [9] C. Xu and F. W. Wise. Recent advances in fibre lasers for nonlinear microscopy. *Nature Photonics*, 7:875 EP –, Oct 2013. Review Article.
- [10] Rafael R. Gattass and Eric Mazur. Femtosecond laser micromachining in transparent materials. *Nature Photonics*, 2:219 EP –, Apr 2008. Review Article.
- [11] X. Liu, D. Du, and G. Mourou. Laser ablation and micromachining with ultrashort laser pulses. *IEEE Journal of Quantum Electronics*, 33(10):1706–1716, Oct 1997.

- [12] U. Keller, D. A. B. Miller, G. D. Boyd, T. H. Chiu, J. F. Ferguson, and M. T. Asom. Solid-state low-loss intracavity saturable absorber for nd:y:lf lasers: an antiresonant semiconductor fabry–perot saturable absorber. *Opt. Lett.*, 17(7):505–507, Apr 1992.
- [13] K. Tamura, H. A. Haus, and E. P. Ippen. Self-starting additive pulse mode-locked erbium fibre ring laser. *Electronics Letters*, 28(24):2226–2228, Nov 1992.
- [14] K. Smith, N. J. Doran, and P. G. J. Wigley. Pulse shaping, compression, and pedestal suppression employing a nonlinear-optical loop mirror. *Opt. Lett.*, 15(22):1294–1296, Nov 1990.
- [15] Sze Y. Set, Hiroshi Yaguchi, Yuichi Tanaka, and Mark Jablonski. Laser mode locking using a saturable absorber incorporating carbon nanotubes. *J. Lightwave Technol.*, 22(1):51, Jan 2004.
- [16] Yu Wang, Sze Y. Set, and Shinji Yamashita. Active mode-locking via pump modulation in a tm-doped fiber laser. *APL Photonics*, 1(7):071303, 2016.
- [17] Shoko Yokokawa, Yu Wang, Sze Y. Set, and Shinji Yamashita. Mode-locked er-doped fiber laser by pump modulation beyond emission lifetime limit. In *Conference on Lasers and Electro-Optics*, page SM4L.1. Optical Society of America, 2017.
- [18] Willis E. Lamb. Theory of an optical maser. *Phys. Rev.*, 134:A1429–A1450, Jun 1964.
- [19] H. A. Haus. Mode-locking of lasers. *IEEE Journal of Selected Topics in Quantum Electronics*, 6(6):1173–1185, Nov 2000.
- [20] M. Bello-Jiménez, C. Cuadrado-Laborde, D. Sáez-Rodríguez, A. Diez, J. L. Cruz, and M. V. Andrés. Actively mode-locked fiber ring laser by intermodal acousto-optic modulation. *Opt. Lett.*, 35(22):3781–3783, Nov 2010.
- [21] M. E. Fermann, F. Haberl, M. Hofer, and H. Hochreiter. Nonlinear amplifying loop mirror. *Opt. Lett.*, 15(13):752–754, Jul 1990.
- [22] Shinji Yamashita. A tutorial on nonlinear photonic applications of carbon nanotube and graphene. *J. Lightwave Technol.*, 30(4):427–447, Feb 2012.
- [23] T. Li. *Optical Fiber Communications: Fiber Fabrication*, volume 1. Academic Press, 1985.
- [24] K. Tamura, E. P. Ippen, H. A. Haus, and L. E. Nelson. 77-fs pulse generation from a stretched-pulse mode-locked all-fiber ring laser. *Opt. Lett.*, 18(13):1080–1082, Jul 1993.
- [25] Andy Chong, Joel Buckley, Will Renninger, and Frank Wise. All-normal-dispersion femtosecond fiber laser. *Opt. Express*, 14(21):10095–10100, Oct 2006.
- [26] J. Freeman and J. Conradi. Gain modulation response of erbium-doped fiber amplifiers. *IEEE Photonics Technology Letters*, 5(2):224–226, Feb 1993.

- [27] M. Murakami, T. Imai, and M. Aoyama. A remote supervisory system based on sub-carrier overmodulation for submarine optical amplifier systems. *Journal of Lightwave Technology*, 14(5):671–677, May 1996.
- [28] K. Shimizu, T. Mizuochi, and T. Kitayama. Supervisory signal transmission experiments over 10000 km by modulated ase of edfas. *Electronics Letters*, 29(12):1081–1083, June 1993.
- [29] S. Novak and A. Moesle. Analytic model for gain modulation in edfas. *Journal of Lightwave Technology*, 20(6):975–985, June 2002.